© 2019. Published by The Company of Biologists Ltd | Development (2019) 146, dev172460. doi:10.1242/dev.172460

STEM CELLS AND REGENERATION

RESEARCH ARTICLE

mTOR controls embryonic and adult myogenesis via mTORC1

Nathalie Rion, Perrine Castets, Shuo Lin, Leonie Enderle*, Judith R. Reinhard, Christopher Eickhorst‡ and Markus A. Rüegg§

ABSTRACT

The formation of multi-nucleated muscle fibers from progenitors requires the fine-tuned and coordinated regulation of proliferation, differentiation and fusion, both during development and after injury in the adult. Although some of the key factors that are involved in the different steps are well known, how intracellular signals are coordinated and integrated is largely unknown. Here, we investigated the role of the cell-growth regulator mTOR by eliminating essential components of the mTOR complexes 1 (mTORC1) and 2 (mTORC2) in mouse muscle progenitors. We show that inactivation of mTORC1, but not mTORC2, in developing muscle causes perinatal death. In the adult, mTORC1 deficiency in muscle stem cells greatly impinges on injury-induced muscle regeneration. These phenotypes are because of defects in the proliferation and fusion capacity of the targeted muscle progenitors. However, mTORC1-deficient muscle progenitors partially retain their myogenic function. Hence, our results show that mTORC1 and not mTORC2 is an important regulator of embryonic and adult myogenesis, and they point to alternative pathways that partially compensate for the loss of mTORC1.

This article has an associated 'The people behind the papers' interview.

KEY WORDS: Raptor, Rictor, Protein synthesis, Satellite cells, Muscle regeneration, Rapamycin

INTRODUCTION

Myogenesis is a tightly controlled process that results in the formation of skeletal muscle in several distinct myogenic waves. During development, mesodermal progenitors that express the paired box protein-3 and -7 (Pax3 and Pax7) give rise to myoblasts, which successively express a set of myogenic regulatory factors [MRFs; such as Myf5, MyoD (Myod1) or myogenin], fuse and differentiate into post-mitotic multi-nucleated muscle fibers (Deries and Thorsteinsdóttir, 2016). Whereas the embryonic wave gives rise to primary myofibers, the fetal wave, starting at around embryonic day (E) 14.5 in mouse, generates secondary myofibers (Biressi et al., 2007). Many of the mechanisms of embryonic myogenesis are recapitulated during muscle regeneration upon injury in the adult. Adult myogenesis relies on quiescent Pax7-positive muscle stem cells, called satellite cells, that become activated and, through multiple differentiation and fusion steps, ensure efficient muscle repair (Dumont et al., 2015).

The mammalian (or mechanistic) target of rapamycin (mTOR) is a protein serine/threonine kinase that assembles into two structurally and functionally distinct multi-protein complexes, mTOR complex 1 (mTORC1) and mTOR complex 2 (mTORC2), which contain the essential components raptor and rictor, respectively (Saxton and Sabatini, 2017). Whereas mTORC1 senses nutrients and growth factors and functions as a central regulator of cell growth by balancing protein synthesis and protein degradation, mTORC2 controls cytoskeletal remodeling, cell metabolism and survival (Saxton and Sabatini, 2017). Although whole-body knockouts of *Mtor*, *Rptor* or *Rictor* in mice are all embryonic lethal (Gangloff et al., 2004; Guertin et al., 2006; Murakami et al., 2004), the phenotypes that are caused by tissue-specific ablations of these genes largely differ between tissues. In skeletal muscle, loss of *Rptor* and *Mtor* causes very similar phenotypes that are dominated by muscle atrophy and a severe myopathy that results in early death of the mice (Bentzinger et al., 2008; Risson et al., 2009). In contrast, skeletal muscle-specific *Rictor* knockout mice do not display any overt phenotype, but their muscles show metabolic changes, such as a greater reliance on lipids and an increased lipid content (Kleinert et al., 2016).

In the past, mTOR signaling has frequently been investigated using its name-giving inhibitor rapamycin. Rapamycin selectively blocks TORC1 in yeast, but also inhibits mTORC2 activity in mammalian cells upon prolonged exposure (Sarbassov et al., 2006). Therefore, genetic modifications are better suited in teasing apart differential functions of mTORC1 and mTORC2. Short-term application of rapamycin was shown to inhibit proliferation of C2C12 myoblasts before differentiation (Conejo and Lorenzo, 2001). On the other hand, rapamycin treatment does not affect satellite cell proliferation after freeze-injury in adult mice (Miyabara et al., 2010). In addition, rapamycin has been reported to interfere with fusion of cultured C2C12 myoblasts (Coolican et al., 1997; Cuenda and Cohen, 1999; Pollard et al., 2014). This 'rapamycin-inhibited' role of mTOR in early differentiation is independent of its kinase domain and has been postulated to be based on mTOR-dependent regulation of IGF2 expression (Erbay and Chen, 2001; Erbay et al., 2003). However, fusion and maturation of myotubes require the kinase activity of mTOR *in vitro* and *in vivo* (Ge et al., 2009; Park and Chen, 2005). The lack of selectivity of rapamycin makes it difficult to conclude that the reported effects are solely based on mTORC1 activity, especially as mTORC2 has also been implicated in myoblast fusion *in vitro* but not *in vivo* (Ge et al., 2011; Pollard et al., 2014; Hung et al., 2014). Hence, the physiological roles of mTORC1 and mTORC2 during embryonic and adult myogenesis remain unclear.

Here, we developed mouse lines that separately delete *Rptor* and *Rictor* in embryonic and adult muscle progenitors. We found that inactivation of mTORC1, but not of mTORC2, affects muscle development and results in perinatal lethality due to respiratory failure. Similarly, selective inactivation of mTORC1 (by *Rptor* deletion) in adult satellite cells results in a severe deficit in muscle regeneration after cardiotoxin (ctx)-induced muscle injury. The myogenic phenotypes that are caused by the loss of mTORC1

Biozentrum, University of Basel, CH-4056 Basel, Switzerland.
*Present address: Toronto Recombinant Antibody Centre/The Donnelly Centre, University of Toronto, Toronto, ON M5G 1L6, Canada. ‡Present address: Institute of Biochemistry II, School of Medicine, Goethe University, 60598 Frankfurt am Main, Germany.

§Author for correspondence (markus-a.ruegg@unibas.ch)

M.A.R., 0000-0002-4974-9384

Received 4 October 2018; Accepted 4 March 2019

Development (2019) 146, dev172460. doi:10.1242/dev.172460

signaling are paralleled by defects of raptor-depleted myoblasts to proliferate and differentiate in culture. Importantly, we also show that raptor-depleted muscle precursors are still able to form myofibers despite the impairment in myogenesis. Our data thus demonstrate an important contribution of mTORC1 and not of mTORC2 to embryonic and adult myogenesis, and they unveil the existence of alternative pathways that can compensate for the loss of mTORC1.

RESULTS

Depletion of raptor impairs muscle development

Recent evidence has indicated that mTORC1 becomes activated in adult satellite cells upon injury (Rodgers et al., 2014). As the activation state of mTORC1 during embryonic myogenesis is unknown, we first stained cross-sections of mice at embryonic day 11.5 (E11.5) for the phosphorylated form of S6, which is indicative of active mTORC1 (Saxton and Sabatini, 2017). The different stages of cell differentiation were distinguished with antibodies to Pax7 (muscle progenitors), MyoD (myoblasts), myogenin (myocytes) and embryonic myosin heavy chain (embMHC, myotubes). Although ∼80% of the Pax7- and MyoD-positive cells were also phospho-S6-positive, only a minority of the myogenin- and almost none of the embMHC-positive cells showed phospho-S6 staining (Fig. 1A-E). These results indicate that mTORC1 activity is high during the proliferative phase of embryonic myogenesis and low during cell fusion and fiber maturation.

To understand the role of mTORC1 and mTORC2 during myogenesis, we generated mice that were deficient for *Rptor* or *Rictor* in skeletal muscle progenitors by crossing *Myf5*–Cre mice (Tallquist et al., 2000) with mice that carried floxed alleles for *Rptor* or *Rictor* (Bentzinger et al., 2008). The *Myf5* gene starts to be expressed in skeletal muscle progenitors at E8 (Ott et al., 1991). Mice that express Cre and are homozygous for the floxed *Rptor* allele ($Myf5^{+/Cre}$; $Rptor^{fl/fl}$), herein called RAmyfKO (for raptor-Myf5-knockout), were born at the expected Mendelian ratio but died immediately after birth (Fig. 2A). In contrast, RImyfKO mice (for rictor-Myf5-knockout; $Myf5^{+/Cre}$; $Rictor^{fl/fl}$) were viable and showed a normal overall muscle histology at young age (Fig. 2B). The cyanotic appearance of the dead RAmyfKO mice suggested a failure to breathe. Indeed, lungs from mutant mice were not inflated and their diaphragm muscle was thinner than in controls (Fig. S1A). In addition, neuromuscular junctions did not form properly, with motor axons overshooting the sites of high acetylcholine receptor (AChR) density (Fig. S1B,C). Moreover, many AChR clusters not in contact with motor nerves were visible in RAmyfKO embryos (Fig. S1C), which is a common phenotype in mice with aberrant neuromuscular junction formation (Tintignac et al., 2015). These results suggested a role of mTORC1 but not mTORC2 in embryonic myogenesis.

We next examined raptor mutant embryos at different stages. As early as E13.5, body weight of RAmyfKO embryos was significantly lower than that of controls (Fig. 2C). Embryos that were heterozygous for the targeted *Rptor* allele ($Myf5^{+/Cre}$; $Rptor^{+/fl}$; termed Het-RAmyfKO) showed no change in body weight and could not be distinguished from controls (Fig. S2A). The weight reduction of E18.5 RAmyfKO embryos was not accompanied by an overall reduction in body size (Fig. S2B) or in the length of the long bones (Fig. S2C) compared with control littermates. Only the rib cage was obviously smaller in RAmyfKO embryos (Fig. S2B), which may be caused by changes in the development of the myotome (Vinagre et al., 2010). Although the different muscle groups had formed in E18.5 RAmyfKO embryos, they were clearly smaller than in controls

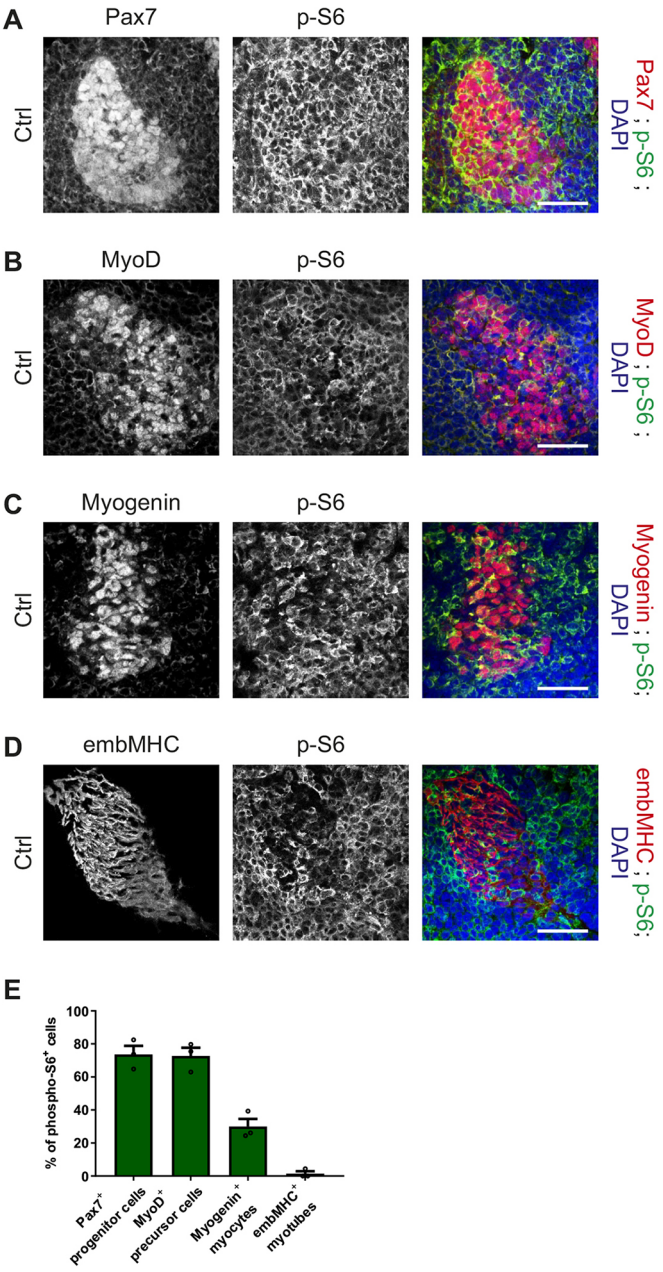

Fig. 1. Activation status of mTORC1 during embryonic myogenesis. (A-D) Immunostaining against phospho-S6 Ser235/236, an indicator of mTORC1 activity, and Pax7 (A), MyoD (B), myogenin (C) and embMHC (D) on cross-sections of control (Ctrl) embryos at E11.5. (E) Percentage of phospho-S6-positive cells in the population of muscle progenitors ($Pax7^+$), precursors ($MyoD^+$), myocytes ($myogenin^+$) and myotubes ($embMHC^+$) (n=3). Data are mean±s.e.m. Scale bars: 50 µm.

(Fig. 2D,E). Moreover, RAmyfKO embryos showed a more pronounced accumulation of fat droplets in muscle (Fig. 2F). Interestingly, at E18.5, mRNA levels of all MRFs, except *Myf5*, were similar in muscle tissues of RAmyfKO and control embryos (Fig. 2G). Similarly, expression of skeletal muscle markers, such as *Myh3* (which encodes embryonic myosin heavy chain) and *Des* (which encodes desmin), was unaltered in mutant embryos (Fig. 2G). The 50% reduction in *Myf5* expression in muscle from E18.5 RAmyfKO embryos was most probably based on the inactivation of one copy of the *Myf5* gene, as its expression is also lower in Het-RAmyfKO embryos (Fig. S2D). In contrast, the effect on muscle

Development (2019) 146, dev172460. doi:10.1242/dev.172460

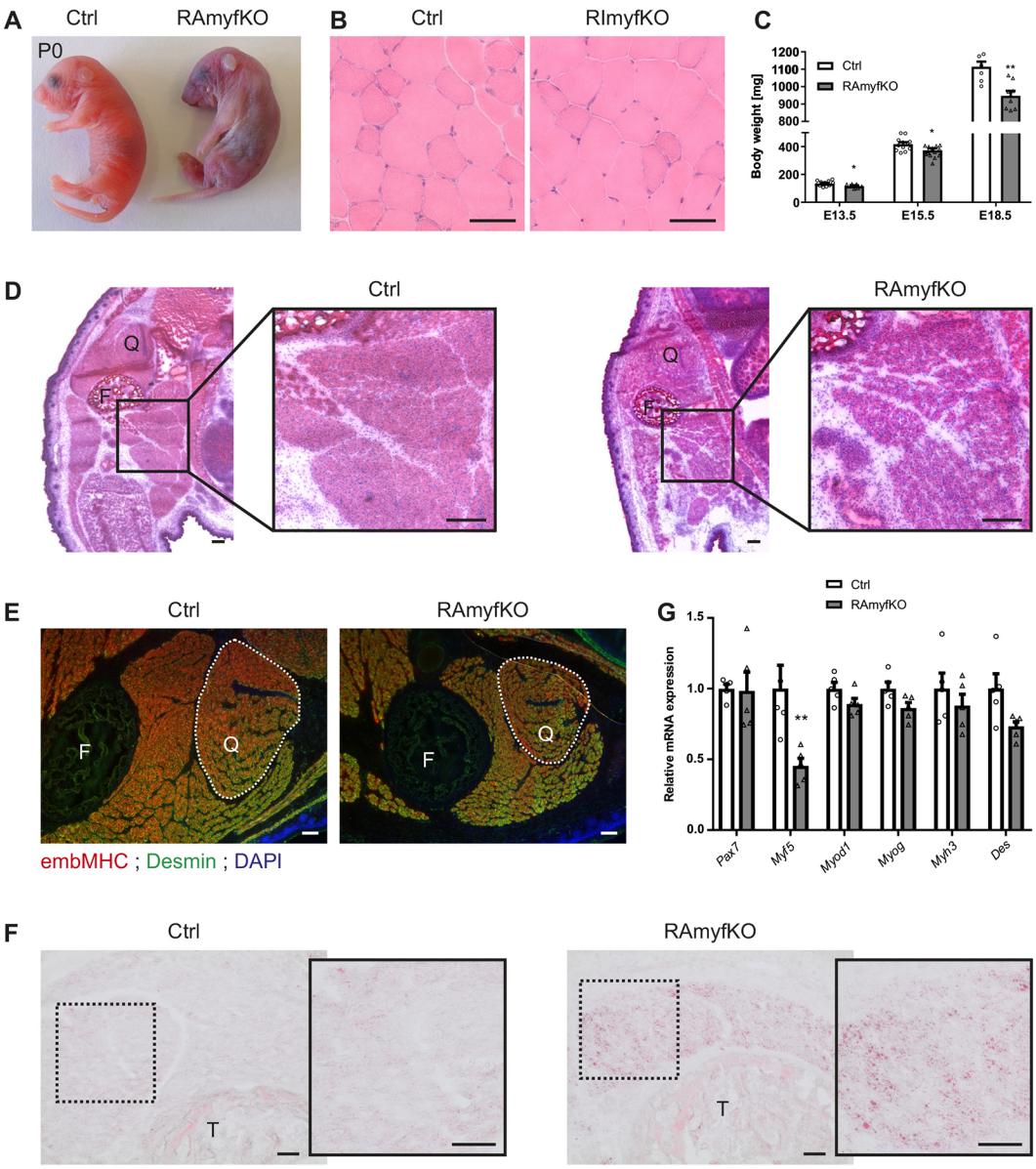

Fig. 2. Ablation of raptor severely impairs embryonic muscle development. (A) Photograph of control (Ctrl) (*Myf5*$^{+/+}$; *Rptor*$^{fl/fl}$) and RAmyfKO (*Myf5*$^{+/Cre}$; *Rptor*$^{fl/fl}$) pups at postnatal day (P) 0. (B) H&E coloration of TA muscle cross-sections of 2-month-old Ctrl (*Myf5*$^{+/+}$; *Rictor*$^{fl/fl}$) and RImyfKO (*Myf5*$^{+/Cre}$; *Rictor*$^{fl/fl}$) mice. (C) Body weight of Ctrl and RAmyfKO embryos at the indicated ages (n=11/12/7 for Ctrl and 7/15/8 for RAmyfKO embryos at E13.5/15.5/18.5, respectively). (D) H&E coloration of cross-sections of Ctrl and RAmyfKO embryos at E18.5. Magnification of boxed area is shown on the right. (E) Immunostaining against embMHC (red) and desmin (green) of cross-sections of E18.5 Ctrl and RAmyfKO quadriceps muscles. Dotted lines delineate the quadriceps muscle. (F) Oil Red O staining of hindlimb cross-sections of E18.5 Ctrl and RAmyfKO embryos. Fat droplet (red) accumulation is more pronounced in RAmyfKO muscle. Magnification of boxed area is shown on the right. (G) Relative mRNA levels of *Pax7*, *Myf5*, *Myod1*, *Myog*, *Myh3* and *Des* in hindlimbs from E18.5 Ctrl and RAmyfKO embryos. Normalization to *Actb* levels (n=5). Data are mean±s.e.m. *P<0.05, **P<0.01, Student's t-test. See also Figs S1 and S2. F, femur; Q, quadriceps; T, tibia. Scale bars: 50 µm in B,F; 200 µm in D; 100 µm in E.

size in the RAmyfKO mice was due to the depletion of raptor from muscle precursors as skeletal muscle of Het-RAmyfKO and *Myf5*$^{+/Cre}$ embryos was indistinguishable from their respective controls (Fig. S2E,F). These results indicate that mTORC1 inactivation in RAmyfKO embryos impairs but does not abrogate the development of skeletal muscle fibers. Of note, brown adipose tissue, which also expresses *Myf5* (Seale et al., 2008), was strongly reduced in RAmyfKO embryos (Fig. S2G), indicating that raptor depletion in brown adipocytes affects the development of the tissue. Altogether, these data show that the depletion of raptor in muscle progenitors strongly impinges on the development of skeletal muscle fibers, but does not abolish their formation.

mTORC1 inactivation affects the first wave of myogenesis

To understand the muscle defects that were observed in E18.5 RAmyfKO embryos, we examined whether mTORC1 inactivation affected the first wave of myogenesis. At E11.5, the area covered by Pax7-positive progenitors was similar in control and mutant embryos (Fig. 3A). However, there were fewer embMHC-positive myotubes in RAmyfKO embryos than in controls (Fig. 3B). We confirmed that Pax7-positive cells in E11.5 RAmyfKO embryos were negative for phospho-S6 (Fig. S3A,B, compared with Fig. 1). Similarly, little phospho-S6 was seen in MyoD-, myogenin- and embMHC-positive cells of RAmyfKO embryos (Fig. S3B-E). Thus, the vast majority of the muscle cells in E11.5 RAmyfKO embryos are depleted for raptor,

Development (2019) 146, dev172460. doi:10.1242/dev.172460

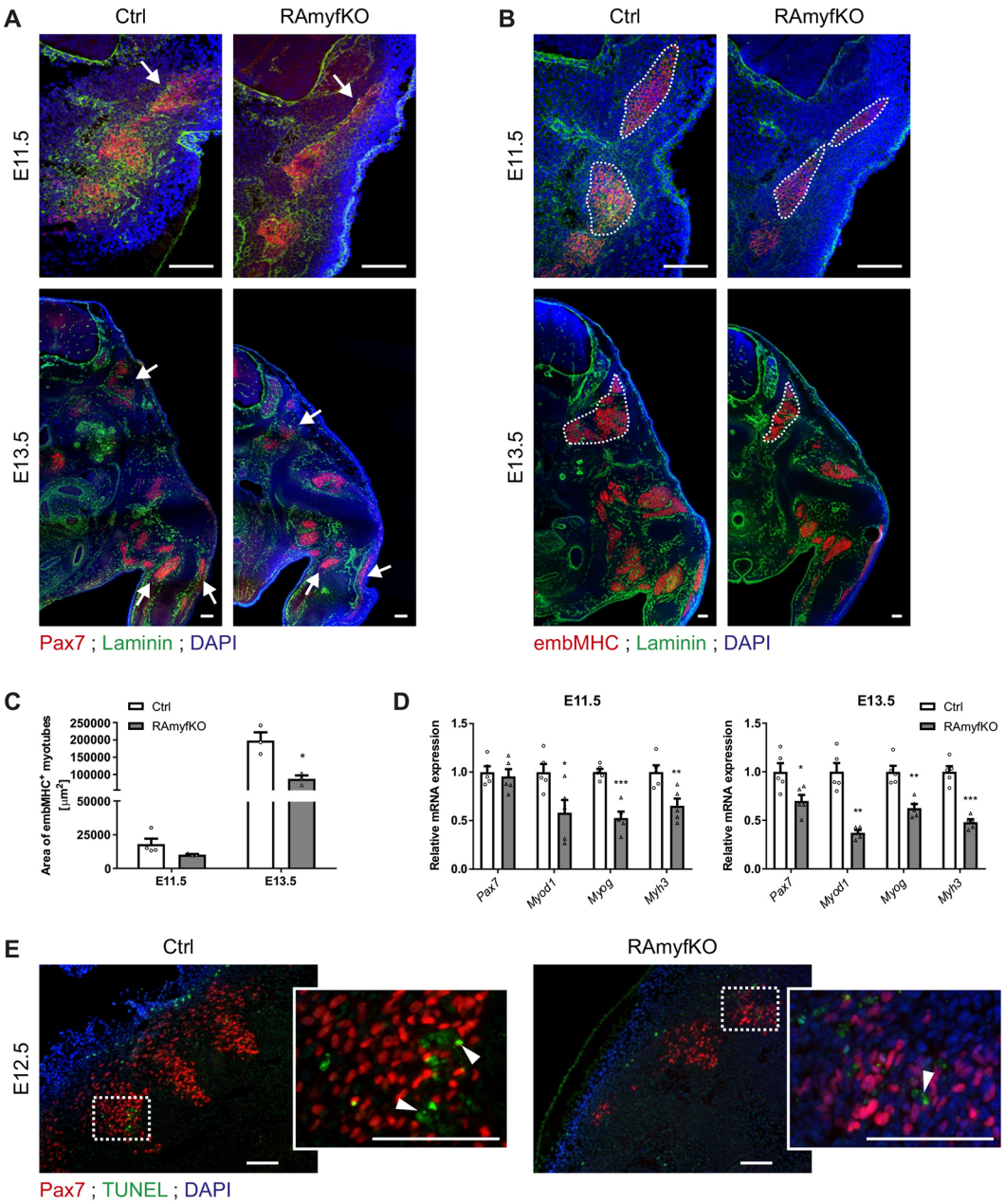

Fig. 3. First wave of myogenesis is altered in the absence of raptor. (A,B) Immunostaining against Pax7 (red, A) or embMHC (red, B) and laminin (green) of cross-sections of E11.5 or E13.5 control (Ctrl) and RAmyfKO embryos. Arrows point to muscle progenitors in the dermomyotome and hindlimbs. The dotted line highlights the myotome, which is formed by primary myotubes. (C) Area of the myotome (embMHC-positive region) in cross-sections of E11.5 and E13.5 Ctrl and RAmyfKO embryos (n=3; except for Ctrl E11.5, n=4). (D) Relative mRNA levels of *Pax7*, *Myod1*, *Myog* and *Myh3* in E11.5 and E13.5 Ctrl and RAmyfKO embryos. Normalization to *Actb* levels (n=5). (E) Immunostaining against Pax7 (red) and TUNEL (green) of cross-sections of E12.5 Ctrl and RAmyfKO embryos. TUNEL-positive nuclei (arrowhead) detected in Ctrl and RAmyfKO embryos did not colocalize with Pax7-expressing progenitors. Magnification of boxed area is shown on the right. Data are mean±s.e.m. *P<0.05, **P<0.01, ***P<0.001, Student's t-test. See also Fig. S3. Scale bars: 100 µm.

suggesting that such cells do contribute to muscle fibers. The trend towards fewer myogenic cells in RAmyfKO embryos became more pronounced at E13.5 and affected both Pax7- and embMHC-positive cells (Fig. 3A,B). At this stage, the size of the myotome, measured by the area of embMHC-positive primary myofibers, was significantly smaller in RAmyfKO than in control embryos (Fig. 3C). Consistently, at E11.5 and E13.5, mRNA levels of MRFs and myogenic markers were significantly lower in RAmyfKO embryos than in controls (Fig. 3D). Notably, E13.5 Het-RAmyfKO embryos showed no difference in muscle formation and in the levels of transcripts encoding MRFs when compared with controls (Fig. S3F-I), indicating that *Myf5* haploinsufficiency does not cause defects in early muscle development. These results show that mTORC1 inactivation affects the first wave of myogenesis, but does not completely prevent the formation of primary myofibers. Importantly, the defects observed were not due to increased apoptosis of raptor-depleted myogenic cells (Fig. 3E). This result indicates that mTORC1-deficient myoblasts are viable and capable of contributing to the muscle lineage, but with markedly lower efficacy.

Development (2019) 146, dev172460. doi:10.1242/dev.172460

RAmyfKO embryos contain myogenic cells that escape Cre-mediated raptor depletion

To assess that raptor-depleted progenitors contributed to the formation of secondary myofibers in E18.5 RAmyfKO embryos, we used EGFP reporter mice, called mR26CS^{EGFP} (Tchorz et al., 2012). Whereas hindlimb muscle of control embryos (*Myf5*$^{+/+}$; *Rptor*$^{fl/fl}$; *mR26CS*$^{EGFP/+}$) did not express EGFP, all muscle fibers in Het-RAmyfKO embryos (*Myf5*$^{Cre/+}$; *Rptor*$^{fl/+}$; *mR26CS*$^{EGFP/+}$) were positive for EGFP (Fig. 4A). The intensity of the EGFP staining varied between muscle fibers in Het-RAmyfKO muscle (Fig. 4A). Interestingly, in hindlimb muscle of RAmyfKO embryos (*Myf5*$^{Cre/+}$; *Rptor*$^{fl/fl}$; *mR26CS*$^{EGFP/+}$), only around half of the fibers expressed EGFP strongly (Fig. 4A). Notwithstanding, some fibers were negative for EGFP, indicating that they had never expressed the Cre recombinase and thus continue to express raptor. In control embryos, high phospho-S6 immunoreactivity was seen in few muscle fibers (Fig. 4B, arrowheads). In RAmyfKO embryos, myofibers with strong EGFP staining (RAmyfKO EGFP^{high}) appeared to be negative for phospho-S6 staining (Fig. 4B; asterisks), whereas muscle fibers with weak EGFP staining (RAmyfKO EGFP^{low}) were often phospho-S6 positive (Fig. 4B; arrowheads). Quantification showed that the difference in phospho-S6 staining in RAmyfKO embryos was highly significant when comparing EGFP^{high} with EGFP^{low} myofibers (Fig. 4C). To see whether depletion of raptor and thus inactivation of mTORC1 would alter mTORC2 signaling, we also examined the activation state of protein kinase Cα, which is a bona fide mTORC2 target. As shown in Fig. 4D and Table S1, both phosphorylation at Ser 657 and the protein levels were unchanged in RAmyfKO muscle. Thus, as has been previously shown for skeletal muscle fibers depleted of raptor (Bentzinger et al., 2008), there is no compensatory increase in mTORC2 activity. In summary, these results indicate that RAmyfKO embryos contain myofibers depleted for raptor and some that escaped *Myf5*-Cre-mediated recombination.

To separate recombined from non-recombined cells, we next isolated myogenic cells from hind- and forelimbs of E18.5 embryos and determined the proportion of EGFP-positive and -negative cells (Fig. 4E). No recombination was observed in cells from control *Myf5*$^{+/+}$ embryos as all cells were EGFP-negative (Fig. 4F). In Cre-expressing control (Ctrl EGFP^{+}; *Myf5*$^{Cre/+}$; *Rptor*$^{+/+}$; *mR26CS*$^{EGFP/+}$) and Het-RAmyfKO embryos, ∼80% of the sorted cells expressed EGFP (Fig. 4E,F). In stark contrast, only 23% of the myogenic cells that were isolated from RAmyfKO embryos were EGFP-positive (Fig. 4E,F). To test whether EGFP-positive cells also recombined loxP sites at the *Rptor* locus, freshly sorted cells were genotyped using specific primers (see Fig. 4G). As a control (Ctrl EGFP^{-}), we used genomic DNA from myogenic cells that were heterozygous for the floxed *Rptor* allele but did not express Cre. In EGFP-negative myoblasts from Het-RAmyfKO embryos, only the floxed *Rptor* allele (Fig. 4H, PCR P1-P2) but no recombined *Rptor* allele (Fig. 4H, PCR P1-P3) was detected as in genomic DNA from controls. In contrast, EGFP-positive myoblasts from Het-RAmyfKO and RAmyfKO embryos were negative for the floxed *Rptor* allele but positive for the *Rptor* allele after recombination (Fig. 4H, PCR P1-P3). The band that corresponds to the recombined *Rptor* allele in RAmyfKO EGFP-negative myoblasts (Fig. 4H) is probably because of contamination by some EGFP-positive cells. Hence, the expression of EGFP in RAmyfKO embryos is a reliable marker for successful recombination of the floxed *Rptor* allele. The increased proportion of non-recombined myoblasts in E18.5 RAmyfKO embryos points to a competitive disadvantage of raptor-depleted myogenic cells.

Loss of mTORC1 slows down, but does not abolish, proliferation and differentiation of myoblasts

To determine the stages of myogenesis that require functional mTORC1, EGFP-positive and -negative cell populations were FACS-isolated, plated at the same density and cultured under growth conditions for 2 days. As mTORC1 is a key regulator of translation initiation, we measured the rate of protein synthesis using the surface sensing of translation (SUnSET) method, which uses the incorporation of puromycin as a readout (Goodman and Hornberger, 2013). EGFP-positive myoblasts from Het-RAmyfKO embryos incorporated puromycin to a similar extent as control cells (EGFP-negative), whereas puromycin incorporation was significantly lower in EGFP-positive myoblasts that were isolated from RAmyfKO embryos (Fig. 5A,B). Moreover, after 48 h in culture, a pulse assay with 5-bromo-2′-deoxyuridine (BrdU) revealed a more than 50% reduction in proliferation of EGFP-positive RAmyfKO myoblasts, compared with control cells (Fig. 5C,D). To examine the ability of raptor-depleted cells to transit from proliferation to differentiation and then fuse, myoblasts were switched from proliferation to differentiation medium. Fourteen hours after this medium change, only ∼4% of the cells were still proliferating, irrespective of the genotype (Fig. 5E). However, after 72 h, fusion of EGFP-positive RAmyfKO myoblasts was limited compared with control cells (Fig. 5F), which was reflected by their significantly lower fusion index (Fig. 5G). In Het-RAmyfKO, EGFP-positive cells did not show any difference in the fusion index compared with controls (Fig. 5G), indicating that *Myf5* haploinsufficiency does not affect the fusion of myoblasts. Although differentiation of EGFP-positive RAmyfKO myoblasts was impaired, some myotubes with a low number of nuclei still formed (Fig. 5H). This phenotype was specific to mTORC1 function, as no deficits in proliferation and differentiation were observed in rictor-depleted (i.e. mTORC2-deficient) myoblasts isolated from 2- to 3-week-old RImyfKO mice (Fig. S4A-G, Table S2). These results show that inactivation of mTORC1, but not of mTORC2, interferes with, but does not completely prevent, myoblast proliferation and differentiation. Based on the puromycin experiment, this defect is likely because of limited protein synthesis, which is consistent with the view that both processes require active protein synthesis (Pallafacchina et al., 2013).

mTORC1 signaling in adult muscle stem cells

To determine whether mTORC1 deregulation also affects muscle stem cell function in the adult, and thereby muscle regeneration, we generated a new mouse model (*Pax7*$^{Cre\text{-}ERT2/+}$; *Rptor*$^{fl/fl}$; *mR26CS*$^{EGFP/EGFP}$), herein called RAscKO (for raptor satellite cell knockout). In these animals, recombination of the floxed *Rptor* alleles and the expression of EGFP reporter are induced in quiescent satellite cells by tamoxifen (tmx) injections. Mice were analyzed 10 or 90 days after tmx treatment (Murphy et al., 2011) (Fig. 6A). No EGFP staining (i.e. no recombination) was detected in mice without tmx treatment or with no Cre expression (Fig. S5A). In contrast, strong EGFP expression was observed 10 days after tmx treatment in Pax7-positive satellite cells of RAscKO mice (Fig. 6B). Quantification by FACS showed that ∼86% of the isolated myogenic cells expressed EGFP (Fig. S5B). As in RAmyfKO myoblasts, PCR on genomic DNA that was isolated from EGFP-positive satellite cells showed successful recombination of the floxed *Rptor* alleles in RAscKO cells (Fig. S5C). Interestingly, mTORC1 inactivation did not significantly alter the number of Pax7-positive satellite cells in tibialis anterior (TA) muscle from RAscKO mice 10 or 90 days after tmx treatment (Fig. 6C,D). These data indicate that mTORC1 activity is dispensable for the

Development (2019) 146, dev172460. doi:10.1242/dev.172460

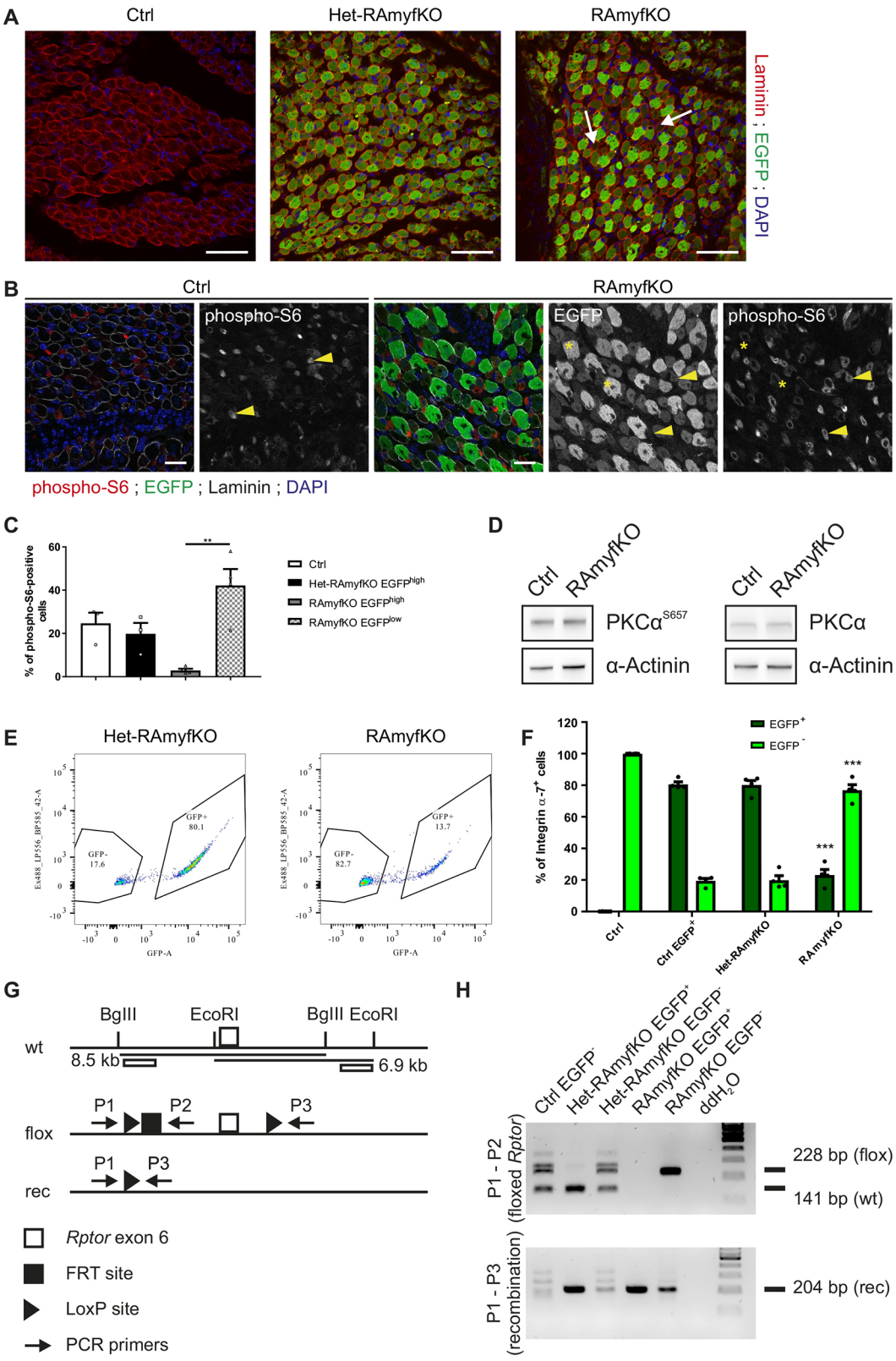

Fig. 4. See next page for legend.

maintenance of the satellite cell pool under homeostatic conditions for up to 3 months.

To test the consequences of mTORC1 inactivation on the regenerative capacity of satellite cells, ctx was injected into the TA and extensor digitorum longus (EDL) muscles of one leg of control and RAscKO mice, seven days after the first tmx injection. One group of mice was re-injured 24 days after the first injury. Muscles were examined 15 or 21 days post-injury (see Fig. 6E). The mass

Development (2019) 146, dev172460. doi:10.1242/dev.172460

Fig. 4. Myogenesis defect caused by mTORC1 inactivation in the Myf5-lineage is partially compensated by non-recombined myoblasts. (A) Immunostaining against laminin (red) and green fluorescent protein (EGFP, green) of E18.5 hindlimb cross-sections. Arrows point to EGFP-negative myofibers detected in RAmyfKO muscles. (B) Immunostaining against phospho-S6 Ser235/236 (red), EGFP (green) and laminin (gray) on hindlimb cross-sections of E18.5 embryos. Phospho-S6 immunoreactivity in muscle fibers is indicated by arrowheads. In RAmyfKO mice, high phospho-S6 does not colocalize with EGFP (asterisks) but is observed in EGFP-negative cells (arrowheads). (C) Quantification of the percentage of phospho-S6-positive muscle fibers [*n*=3 for control (Ctrl) and Het-RAmyfKO; *n*=4 for RAmyfKO embryos]. (D) Western blot analysis of E18.5 Ctrl and RAmyfKO hindlimb muscles using antibodies against the proteins indicated. RAmyfKO muscle shows similar mTORC2 downstream signaling as in controls. α-Actinin was used as loading control (*n*=6 Ctrl; *n*=5 and 6 RAmyfKO for PKCα and p-PKCα, respectively). (E,F) Representative FACS blots of myogenic cells (integrin $\alpha7^+$/$CD45^-$/$CD11b^-$/$Sca1^-$/$CD31^-$) isolated from foreleg and hindlimb muscles of E18.5 Het-RAmyfKO and RAmyfKO embryos and analyzed on their EGFP expression (E). The percentage of EGFP-positive and EGFP-negative cells (F) was normalized to the total number of integrin α7-positive myoblasts (*n*=4; except for Ctrl *n*=8). (G) Scheme of wild-type, floxed and recombined alleles of *Rptor*. Primers used for PCR are indicated as P1, P2 and P3. (H) PCR analysis of FACS-isolated myogenic cells using the indicated primer pairs. The size of the expected products for the different *Rptor* alleles is indicated. Control cells (Ctrl $EGFP^-$) do not express Cre and are heterozygous for the floxed *Rptor* allele ($Myf5^{+/+}$; $Rptor^{fl/+}$; $mR26CS^{EGFP/+}$). EGFP-positive myogenic cells from RAmyfKO mice are only positive for the recombined *Rptor* allele (*n*=3). Data are mean±s.e.m. $^{**}P<0.01$, $^{***}P<0.001$, one-way ANOVA with Tukey's multiple comparisons test or two-way ANOVA with Sidak's multiple comparisons test. See also Table S1. flox, floxed allele containing loxP sites; rec, *Rptor* alleles after recombination by Cre; wt, wild-type allele of *Rptor*. Scale bars: 50 µm in A; 20 µm in B.

ratios between the muscles from the injured and the contralateral non-injured leg were measured as a first readout. This ratio was significantly reduced in RAscKO mice compared with controls (Fig. 6F). Whereas histology of the contralateral muscle (CLM) was similar in control and RAscKO mice (Fig. 6G), the difference was striking in the injured muscles. Control muscle showed complete regeneration, with large centronucleated myofibers 15 days post-injury (1× ctx, 15d). In contrast, only few small regenerating myofibers were present 15 or 21 days post-injury in RAscKO mice (Fig. 6G and Fig. S6A). Consistent with the poor regeneration, RAscKO muscle showed accumulation of collagens (Sirius Red, indicative of fibrosis) and lipids (Oil Red O) (Fig. 6H). Notwithstanding, the presence of some centrally nucleated myofibers in RAscKO mice suggested that raptor-depleted satellite cells can still contribute to the formation of new muscle fibers. Notably, although almost all myofibers in injured control muscle were embMHC-negative 15 days post-injury, most fibers in RAscKO muscle were embMHC- and EGFP-positive at 15 and 21 days after injury (Fig. 6I). Moreover, many Pax7-positive cells remained in the interstitial space in RAscKO muscle 21 days post-injury as compared with controls (Fig. S6B,C). These data indicate that, similar to embryonic muscle progenitors, raptor-depleted satellite cells retain their myogenic function and can still form myofibers, although with a greatly reduced efficacy. Strikingly, after two consecutive rounds of degeneration and regeneration (2×ctx, 15d), RAscKO muscle was largely replaced by fat and fibrotic tissues (Fig. S6D) and only few embMHC-positive fibers could be detected (Fig. S6E). These results demonstrate that mTORC1 signaling in satellite cells is essential for proper regeneration of muscle fibers. Importantly, in RImyfKO muscles, which are deficient of mTORC2 signaling, regeneration was as efficient as in controls (Fig. S6F,G, Table S3). Similarly, mice with a deletion of one *Myf5* allele ($Myf5^{+/Cre}$) did not show any defects in muscle regeneration after two consecutive rounds of ctx-induced injuries (Fig. S6H). These results show that mTORC1, and not mTORC2, is required for efficient muscle regeneration.

Interestingly, skeletal muscles of Het-RAmyfKO mice, although the levels of phospho-S6 and phospho-4E-BP1 tended to be reduced (Fig. S6I, Table S4), did not show any difference in muscle fiber regeneration compared with controls (Fig. S6J,K). Moreover, the number of satellite cells in the injured and non-injured muscles was the same in Het-RAmyfKO and control mice (Fig. S6L,M). Thus, lowering mTORC1 activity to approximately half does not affect muscle regeneration.

Raptor depletion delays activation of satellite cells

To examine further the myogenic potential of raptor-depleted satellite cells, we next isolated and cultured single muscle fibers from the EDL muscle of control and RAscKO mice, 90 days after tmx treatment. In RAscKO mice, 98.07±0.50% of Pax7-positive cells also expressed EGFP (*n*=5, 20-30 myofibers per animal). At time zero (T0), the number of Pax7-positive cells per myofiber in RAscKO mice was not significantly different from that in controls (Fig. 7A). Moreover, at T0, Pax7-positive satellite cells from control and RAscKO mice did not express MyoD (Fig. 7A, see quantification in 7C) and showed very low S6 phosphorylation (Fig. S7A). After 24 h in culture (T24 h), control satellite cells were activated, as shown by the expression of MyoD (Fig. 7B,C). In contrast, 20% of RAscKO satellite cells were Pax7-positive, but remained MyoD-negative (Fig. 7C). All MyoD/Pax7-positive RAscKO satellite cells were phospho-S6-negative, whereas activated control cells turned strongly positive for phospho-S6 (Fig. S7B). At 72 h (T72 h), fibers from control mice were populated by three different myogenic cells, i.e. cells ($Pax7^+$; $MyoD^-$) that returned back to quiescence, activated satellite cells ($Pax7^+$; $MyoD^+$) and committed myoblasts ($Pax7^-$; $MyoD^+$). In contrast, most myogenic cells from RAscKO muscle remained activated ($Pax7^+$; $MyoD^+$), with only a small proportion of quiescent or committed cells (Fig. 7C,D). Importantly, the total number of myogenic cells increased exponentially in fibers that were isolated from control muscle, whereas it remained low in fibers that were isolated from RAscKO mice (Fig. 7E). Notwithstanding, colonies of cells that formed in RAscKO culture after 96 h (T96 h) contained quiescent satellite cells and committed myoblasts (Fig. S7C). These results show that raptor-depleted satellite cells still commit to the myogenic lineage but with a delay when compared with control cells. To address whether this delay might be based on a reduction in protein synthesis, we incubated freshly isolated myofibers (T0) and myofibers after 6 h in culture (T6 h) with puromycin. Satellite cells from control muscle fibers were negative for puromycin incorporation at T0 and became positive at T6 h (Fig. 7F). In contrast, RAscKO satellite cells showed a significant reduction in the rate of protein synthesis at T6 h compared with controls (Fig. 7F). By using cultures of primary adult muscle progenitors, we confirmed that the proliferation rate of raptor-depleted myoblasts was strongly reduced compared with control cells (Fig. S7D). Further, the fusion of RAscKO cells was limited but not abrogated, which indicates that raptor-depleted myoblasts are capable of forming multi-nucleated myotubes (Fig. S7E). Altogether, these data demonstrate that mTORC1 significantly regulates the activation, proliferation and differentiation of adult muscle stem cells and that alternative pathways do exist that can partially compensate for the loss of mTORC1 signaling.

Development (2019) 146, dev172460. doi:10.1242/dev.172460

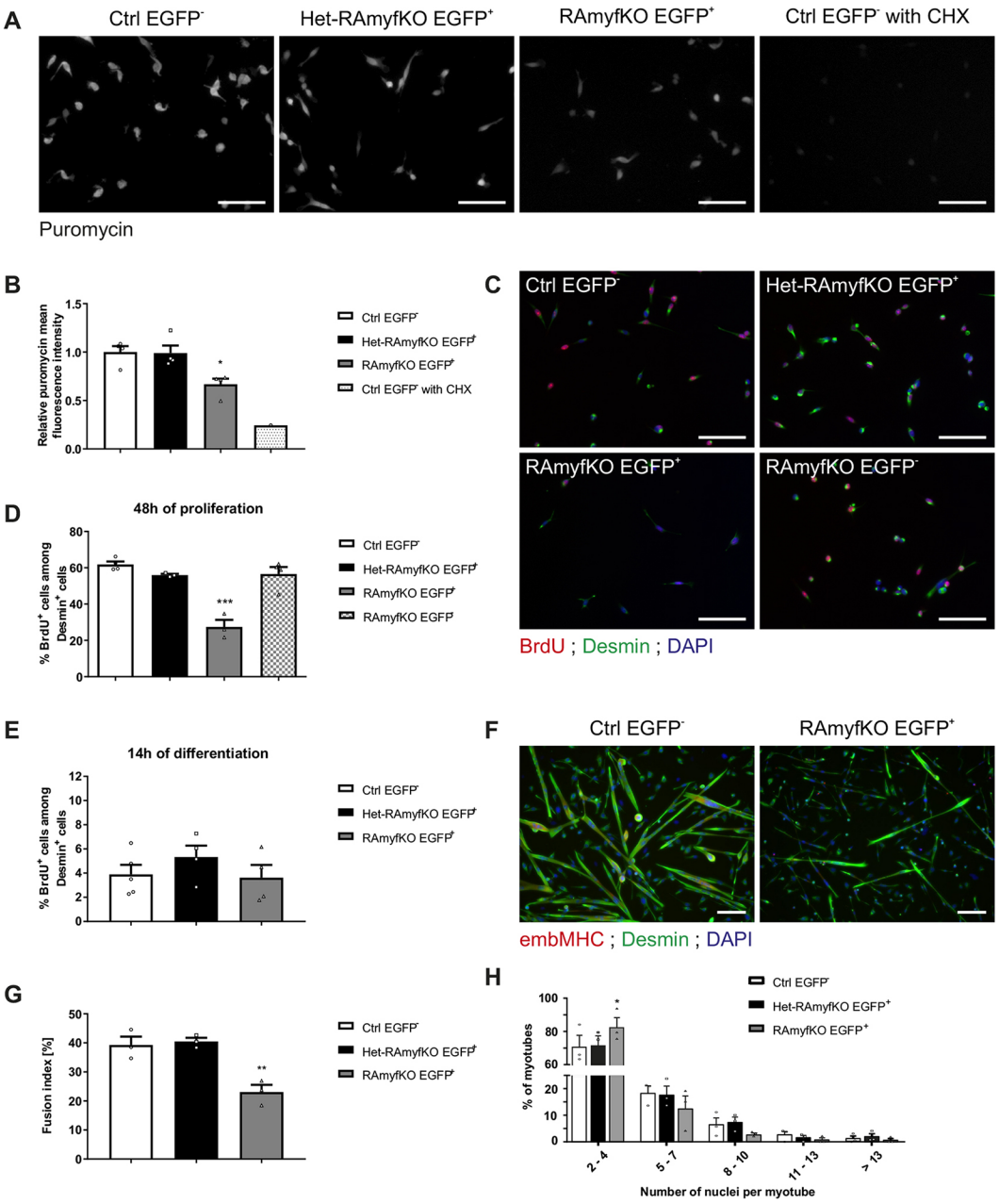

Fig. 5. mTORC1 signaling is crucial for proliferation, differentiation and fusion of embryonic myoblasts *in vitro*. (A) FACS-isolated myogenic cells from E18.5 embryos were plated at the same density and cultured in growth or differentiation media. Cells were cultured in growth media for 48 h and incubated with puromycin only or in combination with cycloheximide (CHX) for 30 min. Puromycin incorporation, an indicator of the rate of protein synthesis, was visualized by immunostaining against puromycin. (B) Mean intensity of puromycin staining normalized to control (Ctrl EGFP^{-}) (n=4). (C) Immunostaining against BrdU (red) and desmin (green) visualizes the myoblasts in the S-phase of the cell cycle during the 1 h BrdU pulse. (D,E) Percentage of BrdU^{+}/desmin^{+} myoblasts after 48 h of proliferation (D; n=3 Ctrl and RAmyfKO EGFP^{-}; n=4 Het-RAmyfKO and RAmyfKO EGFP^{+}) or after 14 h of differentiation (E; n=5 Ctrl; n=4 Het-RAmyfKO and RAmyfKO EGFP^{+}). (F) Immunostaining against embMHC (red) and desmin (green) on myotubes after 3 days of differentiation. (G,H) Fusion index (G) and myotube distribution dependent on the number of myonuclei (H) after 3 days of differentiation (n=3). Data are mean±s.e.m. *P<0.05, **P<0.01, ***P<0.001, one-way ANOVA with Tukey's multiple comparisons test. See also Fig. S4 and Table S2. Scale bars: 100 µm.

DISCUSSION

Our study provides unequivocal evidence that mTORC1 but not mTORC2 is an important regulator of myogenesis. Whereas rictor-deficient muscle progenitors did not show any overt phenotype, the most striking difference between raptor-depleted and control muscle progenitors was their slow proliferation. This became evident in the low BrdU labeling of cultured raptor-deficient embryonic and adult muscle precursor cells, and in the reduced number of myogenic cells that are associated with RAscKO myofibers after 72 h in culture. Such a proliferation deficit upon depletion of raptor is not unprecedented and is the main contributor to the phenotype of raptor-depleted neuronal precursors (Cloetta et al., 2013). Furthermore, mTORC1-dependent changes in proliferation have been reported in β-cells of the pancreas and in mouse embryonic fibroblasts (Blandino-Rosano et al., 2017; Dowling et al., 2010). In mouse embryonic fibroblasts, the change in proliferation by

Development (2019) 146, dev172460. doi:10.1242/dev.172460

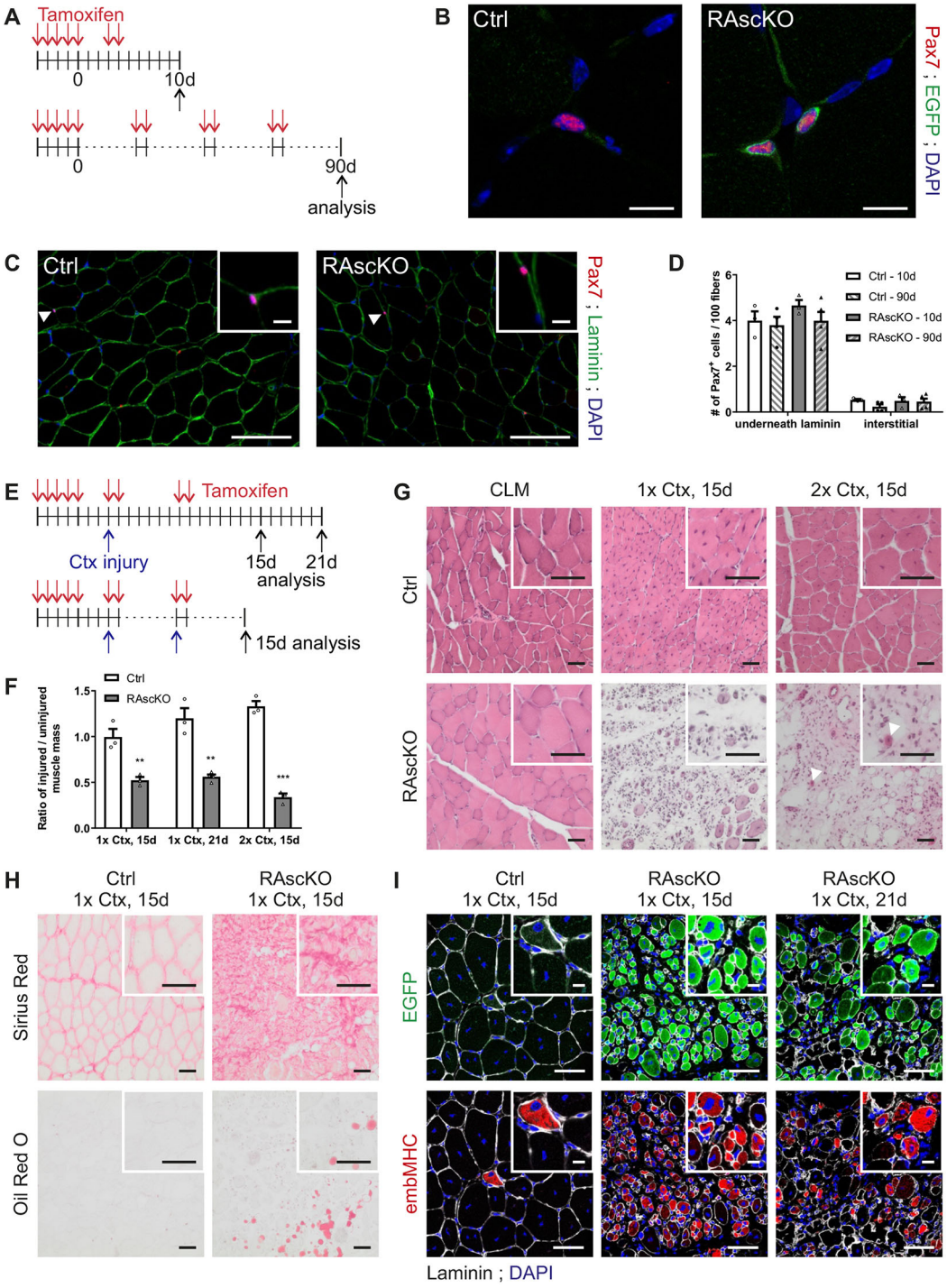

Fig. 6. See next page for legend.

mTORC1 inhibition is mainly due to constitutive inhibition of protein translation by the eukaryotic translation initiation factor 4E-binding proteins (4E-BPs; Dowling et al., 2010), which may increase the time needed for cell cycle progression. mTORC1 remains highly active in the G2/M phase (Bonneau and Sonenberg, 1987), during which cyclin-dependent kinase 1 (CDK1) phosphorylates raptor, which, in turn, promotes IRES-dependent mRNA translation (Ramirez-Valle et al., 2010).

Another observation that suggests a delay in proliferation strongly contributes to the phenotype of RAmyfKO embryos is the increased proportion of cells that are not targeted by Cre-mediated recombination. This increase in the ratio of non-targeted to targeted cells occurred between E11.5 and E18.5. In E11.5 RAmyfKO embryos, many EGFP-positive and phospho-S6-negative cells were observed but only few EGFP-positive cells were left at E18.5. There is evidence that myogenic precursors can escape recombination in *Myf5-Cre* mice (Comai et al., 2014) and that ablation of Myf5-expressing cells allows non-targeted cells to expand and contribute to muscle formation during embryogenesis (Gensch et al., 2008; Haldar et al., 2008). In addition, it has been

Development (2019) 146, dev172460. doi:10.1242/dev.172460

Fig. 6. Raptor depletion strongly impairs regeneration following muscle injury. (A) Experimental scheme for B-D. Three-month-old mice were injected with tmx for 5 consecutive days and muscles were harvested 10 or 90 days post-treatment. In long-term studies, tmx was injected twice every month. (B,C) Immunostaining against Pax7 (red) and EGFP (green, B) or laminin (green, C) on TA muscle cross-sections from 3-month-old control (Ctrl) and RAscKO mice 10 days after tmx treatment. Arrowheads point to quiescent Pax7-positive satellite cells lying underneath the basal lamina. (D) Relative number of Pax7-positive cells per 100 myofibers in TA muscle. Counting was performed 10 or 90 days after tmx treatment (n=3 per group for 10d; n=4 for Ctrl and n=5 for RAscKO mice for 90d). (E) Experimental scheme for F-I. Ctx was injected into TA and EDL muscles of 3-month-old mice at day 7. A subgroup of mice were re-injured 24 days after the first ctx injection. Analysis was performed 15 or 21 days post-injury. The non-injured CLM was used as control. (F) Mass ratio of injured (ctx) and non-injured (CLM) muscles at day 15 or 21 post-injury (n=3; except RAscKO 1× ctx, 21d, n=4). (G) H&E coloration of CLM and injured TA from Ctrl and RAscKO mice, 15 days after one (1× ctx, 15d) or two injuries (2× ctx, 15d). Centralized nuclei are characteristic of regenerating fibers. Arrowheads point to regenerating myofibers found in injured RAscKO muscle. (H) Sirius Red and Oil Red O colorations on regenerating TA muscles from Ctrl and RAscKO mice, 15 days after injury. Injured RAscKO muscle shows accumulations of fibrotic tissue and lipid droplets. (I) Immunostaining against EGFP (green) or embMHC (red) and laminin (gray) on regenerating TA muscle of Ctrl and RAscKO mice, 15 or 21 days post-injury. In regenerating Ctrl muscle only very few embMHC-positive myofibers were detected. Most EGFP-positive myofibers in regenerating RAscKO muscle were also positive for embMHC. Data are mean ±s.e.m. **P<0.01, ***P<0.001, Student's t-test. See also Figs S5 and S6 and Tables S3 and S4. Scale bars: 10 µm in B; 100 µm in C (10 µm in inset); 50 µm in G (50 µm in inset); 50 µm in H (50 µm in inset); 50 µm in I (10 µm in inset).

proposed that one population of Myf5-independent precursor cells solely expresses Pax7 and MyoD during myogenesis (Gensch et al., 2008; Haldar et al., 2008). Hence, the increased proportion of EGFP-negative (i.e. non-targeted) myoblasts that is isolated from E18.5 RAmyfKO compared with control embryos strongly supports the notion that these escaper cells partially compensate for the slow proliferation rate of raptor-depleted cells. It is, however, important to note that raptor deficiency decreases protein synthesis in RAmyfKO myoblasts by less than 50%. Possible compensatory pathways include MAP kinase signaling via its regulatory role on the Mnk1/Mnk2 kinases (Sonenberg and Hinnebusch, 2009). Although the MAPK and mTOR pathways appear to have complementary roles in the control of the overall initiation of protein translation, it is not known whether the different pathways control translation of specific subsets of mRNAs. Thus, loss of mTORC1 may affect translation of particular mRNAs that are essential for efficient cell proliferation.

Raptor-depleted myoblasts are able to fuse and form myofibers

Another important new insight of our work is that mTORC1 depletion does not abolish the capability of myoblasts or satellite cells to fuse and form myofibers. Although the overall efficacy of myofiber formation was reduced, raptor-depleted myoblasts contributed to the myogenic process in E11.5 and E13.5 RAmyfKO embryos. We also detected EGFP-positive myofibers, which lacked S6 phosphorylation and hence mTORC1 activity, in E18.5 RAmyfKO muscles. Similarly, injury-triggered muscle regeneration in adult RAscKO mice still occurred. Finally, myoblasts that were isolated from RAmyfKO embryos or RAscKO mice formed multi-nucleated myotubes *in vitro*. Previous studies have investigated the role of mTORC1 in muscle differentiation by using the mTOR inhibitor rapamycin or expressing mTOR mutants. In these experiments, rapamycin reduced the differentiation capacity of rat and mouse myoblasts *in vitro* and *in vivo* (Ge and Chen, 2012). Whereas this fusion deficit *in vitro* was rescued by the expression of a kinase-dead mutant of mTOR, late-stage differentiation and maturation required the kinase activity of mTOR (Ge et al., 2009; Erbay and Chen, 2001). Although these data predict high mTORC1 activity during differentiation, we found that mTORC1 signaling was low or absent in newly formed myofibers of E11.5 control embryos, suggesting that mTORC1 is not required after the fusion process during the embryonic (first) wave of myogenesis. Interestingly, the increase in muscle size during embryonic development is mainly based on myonuclear accretion, whereas an increase in the myonuclear domain is responsible for later perinatal muscle growth (White et al., 2010). As we show that myofibers do form in the absence of mTORC1 signaling, we hypothesize that the increase in the myonuclear domain might be particularly impaired upon mTORC1 inactivation. In summary, our data provide evidence that mTORC1 signaling has a differential role during skeletal muscle development. Early stages of myogenesis are affected by the delay in proliferation upon mTORC1 inactivation, whereas the late stages may be mainly affected by the lack of sufficient muscle growth after fusion. In contrast, mTORC2 signaling is dispensable for embryonic muscle development.

The role of mTORC1 in quiescent satellite cells and during regeneration

We also used *Pax7*-CreERT2 mice to eliminate raptor from quiescent, adult satellite cells. Consistent with the observation that quiescent satellite cells have low mTORC1 activity (Rodgers et al., 2014), abrogation of raptor for up to 3 months did not alter the size of the stem cell pool under homeostatic conditions. This indicates that the complete loss of mTORC1 signaling does not provoke apoptosis of quiescent satellite cells and that the low level of protein synthesis required for maintaining the satellite cell pool is independent of mTORC1 signaling. This observation is in agreement with the findings that rapamycin or genetic silencing of mTORC1 components resulted in the 'rejuvenation' of senescent satellite cells (Garcia-Prat et al., 2016; Haller et al., 2017). Interestingly, the initiation factor eIF2α is phosphorylated in quiescent satellite cells to inhibit general mRNA translation, and removal of this phosphorylation site is sufficient to drive satellite cells into activation (Zismanov et al., 2016). Thus, suppression of mRNA translation appears to be an important feature to maintain quiescence in satellite cells (Fujita and Crist, 2018). Inversely, induction of protein synthesis is necessary to allow efficient muscle regeneration (Rodgers et al., 2014; Zismanov et al., 2016). Processes that require protein synthesis during regeneration are the expression of Myf5 and MyoD (Zismanov et al., 2016; Crist et al., 2012) and the efficient proliferation of activated satellite cells. Consistent with mTORC1 contributing to this increase in protein synthesis during regeneration, activated satellite cells are marked by high mTORC1 activity and satellite cells that are in an alerted state (G_{Alert}) by a non-muscle injury are more efficient in regenerating skeletal muscle after ctx-induced injury (Rodgers et al., 2014). Although those studies did not directly test the differential function of mTORC1 and mTORC2, we now report a strong deficit in muscle regeneration in the absence of mTORC1, but not of mTORC2 signaling. The deficits are based on the delay in the transition from quiescence into activation, as was seen by the increased proportion of RAscKO satellite cells that lacked MyoD after 24 h in culture. This delayed commitment of RAscKO satellite cells, together with their slow proliferation, were likely responsible for the severe impairment in muscle fiber regeneration after ctx-induced injury in RAscKO mice. Interestingly, large areas were also infiltrated with

Development (2019) 146, dev172460. doi:10.1242/dev.172460

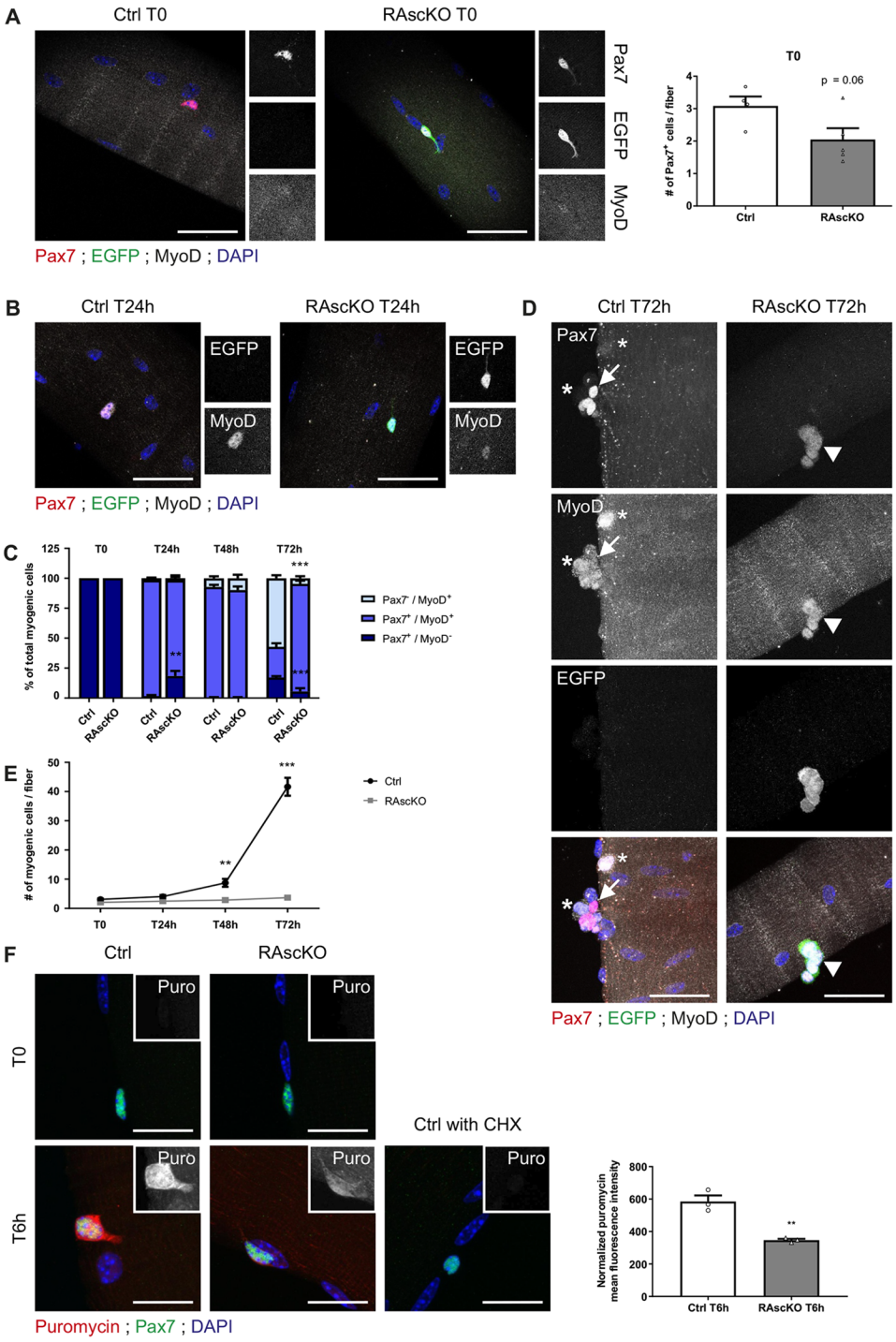

Fig. 7. Loss of mTORC1 delays the activation of satellite cells. (A,B,D) Single myofibers were isolated from control (Ctrl) and RAscKO EDL muscles 90 days after tamoxifen treatment and their associated satellite cells analyzed directly after isolation (T0) or after 24, 48 or 72 h in culture (T24 h, T48 h, T72 h). Immunostaining against Pax7 (red), EGFP (green) and MyoD (gray) on satellite cells at T0 (A), T24 h (B) or T72 h (D). The number of Pax7-positive cells per fiber was counted (A; n=4 Ctrl and n=5 RAscKO mice, 20-30 myofibers per animal). At T24 h, Ctrl satellite cells express MyoD (B; activated state). At T72 h, Ctrl satellite cells (D) have formed clones containing Pax7^{+}/MyoD^{-} (quiescent, arrow) cells, Pax7^{-}/MyoD^{+} (committed, asterisks) cells and Pax7^{+}/MyoD^{+} (activated, arrowhead) cells. (C) Proportion of Pax7- and/or MyoD-positive cells to the total number of myogenic cells on single isolated myofibers at T0, T24 h, T48 h and T72 h (n=4 Ctrl and n=4/5 RAscKO mice, 20-30 myofibers per animal). (E) Number of myogenic cells per fiber at T0, T24 h, T48 h and T72 h (n=4 Ctrl and n=5 RAscKO mice, 20-30 myofibers per animal). (F) Fibers at T0 or T6 h were incubated with puromycin alone or in combination with cycloheximide (CHX) for 30 min. Puromycin incorporation, an indicator of the rate of protein synthesis, was visualized by immunostaining against puromycin. Mean fluorescence intensity of puromycin staining was normalized to the intensity in myofibers (n=3, 25-30 satellite cells per animal). Data are mean±s.e.m. **P<0.01, ***P<0.001, Student's t-test. See also Fig. S7. Scale bars: 50 µm.

collagens and lipids in injured RAscKO muscle, which suggests that fibroblast and adipocyte differentiation further suppressed the regeneration process. Fibroblasts and adipocytes that infiltrate muscle that is undergoing chronic degeneration and regeneration originate from fibro-adipogenic progenitors (FAPs), the differentiation of which is repressed in healthy muscle by the presence of restored myofibers (Mozzetta et al., 2013; Uezumi et al., 2010).

Nevertheless, it is important to note that RAscKO satellite cells still entered the activated state at later time points and also re-entered quiescence after 96 h of culture. Thus, RAscKO satellite cells make use of mTORC1-independent pathways to induce MyoD expression and to renew the satellite pool after injury. Hence, we provide evidence that loss of mTORC1 signaling in satellite cells does not prevent their transition from quiescence into activation, but severely impairs their capacity to regenerate skeletal muscle owing to defects in proliferation.

A possible role of mTORC1 signaling in neuromuscular junction formation and maintenance

In skeletal muscle fibers, mTORC1 is a main determinant of autophagy induction, which may account for the observed myopathies in mice with altered mTORC1 signaling (Bentzinger et al., 2008; Castets et al., 2013; Risson et al., 2009). However, loss of

Development (2019) 146, dev172460. doi:10.1242/dev.172460

autophagy by depleting Myf5-expressing cells of Atg7 does not affect the viability of mice, as well as embryonic muscle development (Martinez-Lopez et al., 2013). Therefore, possible alterations in the autophagy pathway upon mTORC1 inactivation in muscle progenitors is not the main cause for the defects that are observed in myogenesis of RAmyfKO embryos. Because they die of respiratory failure, we also examined the neuromuscular junctions (NMJ) and show significant defects in muscle innervation. Although it remains unclear whether these NMJ changes are a consequence of the incomplete formation of skeletal muscle fibers in RAmyfKO embryos, a direct effect of mTORC1 signaling on the NMJ is feasible. For example, innervation defects in the diaphragm, which results in the appearance of extrasynaptic AChR clusters, have been observed in mice that were depleted for raptor in skeletal muscle fibers (Bentzinger et al., 2008). Moreover, abrogation of autophagy in skeletal muscle also destabilizes NMJs (Carnio et al., 2014).

In conclusion, our data demonstrate that coordinated mTORC1, but not mTORC2, signaling is crucial for the formation of skeletal muscle during embryogenesis and regeneration of the adult tissue. We provide evidence that mTORC1 activity is tightly controlled during the myogenic process and that loss of its signaling strongly affects, but does not abolish, the myogenic function of muscle progenitors. Deregulation of mTORC1 signaling may therefore be a major contributor in the alterations of the myogenic process in muscle pathologies and skeletal muscle aging.

MATERIALS AND METHODS

Mice

RAmyfKO and RAscKO mice were generated by crossing *Rptor*-floxed mice (Bentzinger et al., 2008) with *Myf5*-Cre mice that were obtained from Jackson Laboratories (Tallquist et al., 2000) or mice that expressed Cre-ERT2 in the *Pax7* locus (Murphy et al., 2011), respectively. In addition, both mouse models were crossed with *mR26CS*-EGFP mice (Tchorz et al., 2012). RImyfKO mice were generated by crossing *Rictor*-floxed mice (Bentzinger et al., 2008) with *Myf5*-Cre mice (Tallquist et al., 2000). Genotyping and recombination PCR for the conditional *Rptor* or *Rictor* allele, Cre recombinase knock-in in the *Myf5* or *Pax7* locus and *mR26CS*-EGFP transgene expression was performed as previously described (Tchorz et al., 2012; Bentzinger et al., 2008; Murphy et al., 2011; Tallquist et al., 2000). To induce raptor depletion in Pax7-expressing cells, tmx (2.5 mg/day) diluted in corn oil was injected intraperitoneally in 2- to 3-month-old mice for 5 consecutive days. For the analysis of adult mice, only male mice were used. All mice were maintained in a licensed animal facility with a fixed 12 h dark-light cycle and allowed food and water *ad libitum*. All animal studies were performed under the guidelines and the law of the Swiss authorities and regularly controlled and approved by the veterinary office according to the Swiss Animal Protection Ordinance of 23 April 2008 (AniPO).

Skeleton staining

E18.5 embryos were skinned, macerated and stained with Alcian Blue (cartilage, Sigma-Aldrich) and Alizarin Red (ossified bones, Sigma-Aldrich). The detailed protocol was previously described (Schneider, 2013). The stained skeleton was imaged using a Leica M60 stereomicroscope and a Leica IC80 HD camera.

Cell culture

Isolation of primary muscle progenitors from embryos by FACS was adapted from Pasut et al. (2012). Isolation of adult muscle stem cells from hindlimb and foreleg muscles of 3-month-old mice by FACS was done according to a protocol modified from Garcia-Prat et al. (2016). For further details on FACS isolation procedures, see supplementary Materials and Methods. RImyfKO primary myoblasts were obtained as previously described (Rosenblatt et al., 1995). Primary myoblasts were maintained in Glutamax Dulbecco's modified Eagle's medium (DMEM Glutamax, ThermoFisher Scientific) supplemented with 10% horse serum (HS), 20% fetal bovine serum, 1% chicken embryo extract (CEE), 1% penicillin-streptomycin (pen/strep) and 0.5 ng/ml β-fibroblast growth factor on Matrigel-coated cell culture dishes at 37°C with 5% CO_2. To induce differentiation, an equal number of cells was plated at high density and incubated with DMEM Glutamax containing 4% HS, 1% CEE and 1% pen/strep 1 day after FACS isolation. To test the proliferation capacity of myoblasts, the same number of cells was incubated in proliferation medium for 48 h or in differentiation medium for 12 or 14 h, and 7.67 µg/ml BrdU was added for 1 h. To analyze the rates of protein synthesis, cells were incubated with 1 µM puromycin with or without 100 µg/ml cycloheximide for 30 min. Cells were fixed with 4% paraformaldehyde (PFA), washed with PBS (pH 7.4) and 0.1 M glycine, and kept frozen for subsequent immunostaining.

Ctx injury

Mice were anesthetized by intraperitoneal injection of ketamine (111 mg/kg, Ketalar, Pfizer) and xylazine (22 mg/kg, Xylaxin Streuli, Streuli Pharma). To induce complete muscle necrosis, TA and EDL muscles of one leg were injected with 150 µl of 6.7 µg ctx to induce complete muscle necrosis. The other leg was untreated and served as the contralateral control. Mice were treated with 0.1 mg/kg buprenorphine, twice a day for at least 3 days. The second ctx-injury was induced 24 days after the first injection. TA and EDL muscles were analyzed 15 or 21 days after injury.

Single myofiber culture

Single myofibers were isolated from EDL muscle of 3-month-old mice 10 or 90 days after tmx treatment as previously described (Rosenblatt et al., 1995). Fibers analyzed at T0 were immediately fixed with 4% PFA. Fibers kept in culture for up to 96 h were transferred into DMEM Glutamax, 1% pen/strep, 10% HS, 1% CEE and fixed with 4% PFA at the time points indicated. Some fibers were incubated with 10 µM puromycin with or without 100 µg/ml cycloheximide in DMEM Glutamax at T0 or in DMEM Glutamax containing 1% pen/strep, 10% HS and 1% CEE at T6 h for 30 min and then fixed with 4% PFA. Fibers were washed with PBS, permeabilized with PBS containing 0.5% Triton-X100, washed again and incubated in blocking solution (10% HS, 10% goat serum, 0.35% carrageenan, PBS) for 30 min. Primary antibodies were added overnight at 4°C. Fibers were washed in PBS containing 0.025% Tween-20 and incubated with the secondary antibodies for 1.5 h. Following the washing steps, the fibers were collected with a smoothened, horse serum-coated glass pipette and transferred on Non-Superfrost glass slides (ThermoFisher Scientific) coated with 84% acetone, 16% (3-aminopropyl)triethoxysilane. The fibers were mounted with Vectashield DAPI medium (VectorLabs). Primary antibodies used were: anti-MyoD1 (clone c-20; #sc-304; Santa Cruz; 1:100), anti-Pax7 (supernatant; Developmental Studies Hybridoma Bank; 1:100), anti-puromycin (clone 12D10; MABE343; Millipore; 1:1000), anti-phospho-S6 ribosomal protein (Ser235/236; #4858S; Cell Signaling Technology; 1:200) and anti-GFP tag (#A10262; Thermo Fisher Scientific; 1:400). The secondary antibodies used were: anti-mouse IgG1 Cy3, anti-rabbit A568 and anti-chicken A488 (Jackson ImmunoResearch; 1:300).

Histology

Mouse embryos were isolated at the embryonic stage of interest and equilibrated in 30% sucrose/PBS overnight at 4°C. Embryos were embedded and frozen in Tissue-Tek and serially cut into 12 µm sections. Only sections from embryos that were frozen and cut in the same orientation were compared. Muscles from adult mice were dissected, frozen in liquid nitrogen-cooled isopentane and cryosectioned at 8 µm. Embryos or adult muscles that expressed EGFP were fixed in 4% PFA overnight or in 2% PFA for 2 h, respectively, and were incubated in 20% sucrose overnight before freezing. Histology analysis was performed using Hematoxylin and Eosin (H&E) staining followed by sequential dehydration with 70%, 90%, 100% ethanol and 100% xylene. For Oil Red O staining, sections were fixed with 4% PFA for 1 h, stained with Oil Red O (5 mg/ml in 60% triethyl-phosphate) for 30 min, washed with running tap water and mounted in 10% glycerol. Collagens were stained with a Picro-Sirius Red solution (1 mg/ml in 1.3% aqueous solution of picric acid) for 1 h followed by washing in

Development (2019) 146, dev172460. doi:10.1242/dev.172460

0.5% acidic water for 30 min. The slides were mounted following dehydration in 100% ethanol and after clearing in xylene.

Immunostaining

Cross-sections or cells were fixed with 4% PFA, washed in PBS (pH 7.4), 0.1 M glycine and permeabilized with pre-cooled methanol. Antigen retrieval was achieved by warming the sections in 0.01 M citric acid just below the boiling point. The samples were blocked in 3% IgG-free bovine serum albumin (BSA) supplemented with 0.05 mg/ml AffiniPure Mouse IgG, Fab Fragment (Jackson ImmunoResearch). Primary antibodies were incubated overnight at 4°C. The samples were washed with PBS, incubated with the corresponding secondary antibodies for 1.5 h at room temperature, washed again and mounted with Vectashield DAPI medium. Immunostaining against EGFP and phospho-S6 ribosomal protein (Ser235/236) was performed without methanol treatment and antigen retrieval; instead, 0.5% Triton X-100 was added to the blocking solution. Apoptotic nuclei were immunolabeled using the *In Situ* Cell Death Detection Kit, Fluorescein (Sigma-Aldrich) according to the manufacturer's protocol. Primary antibodies used were: anti-phospho-S6 ribosomal protein (Ser235/236; #4858S; Cell Signaling Technology; 1:200), anti-Pax7 (supernatant; Developmental Studies Hybridoma Bank; 1:50), anti-MyoD1 (clone 5.8A; #554130; BD Biosciences; 1:500), anti-myogenin (supernatant; #f5d; Developmental Studies Hybridoma Bank; 1:50), anti-myosin (embryonic; biosupe; #F1.652; Developmental Studies Hybridoma Bank; 1:1200), anti-desmin (#ab15200; Abcam; 1:300), anti-laminin (#ab11575; Abcam; 1:300), anti-GFP tag (#A10262; Thermo Fisher Scientific; 1:400), anti-BrdU (BU1/75, ICR1; #ab6326; Abcam; 1:500), anti-puromycin (clone 12D10; MABE343; Millipore; 1:1000). The secondary antibodies used were: anti-mouse Biotin, anti-mouse IgG1 Cy3, anti-rabbit A568, anti-chicken A488, anti-rat A568 and streptavidin Cy3 (Jackson ImmunoResearch; 1:1000).

Whole mount immunostaining

Whole-mount immunostaining of diaphragms from E17.5 embryos was performed by fixing the tissue with 1% PFA, 0.1 M sodium phosphate (pH 7.3) at 4°C. The diaphragms were rinsed in PBS, incubated in 0.1 M glycine (pH 7.3) and blocked in 2% BSA, 4% normal goat serum, 0.5% Triton X-100, PBS. The primary antibody was incubated overnight in 2% BSA, 4% normal goat serum, PBS. After washing for 1 h, the secondary antibody was incubated overnight. The washing was repeated and the samples sequentially post-fixed in 1% PFA, 100% methanol and mounted in citifluor. Primary antibodies and the dilution factors used were: anti-synaptophysin (A0010; Dako; 1:200), anti-neurofilament (N4142; Sigma-Aldrich; 1:8000). The secondary antibody used was: anti-rabbit A488 (Jackson ImmunoResearch; 1:1000).

Immunoblotting

The hindlimbs from E18.5 embryos were frozen in liquid nitrogen. Quadriceps and TA muscles from 3- and 5-month-old mice, respectively, were frozen in liquid nitrogen and powdered on dry ice. Proliferating primary myoblasts were collected after trypsinization, washed in cold PBS and snap-frozen as pellets in liquid nitrogen. Samples were lysed in cold RIPA buffer [50 mM Tris-HCl (pH 8), 150 mM NaCl, 1% NP-40, 0.5% sodium deoxycholate, 0.1% SDS, 1% Triton X-100, 10% glycerol, ddH_2O] supplemented with phosphatase and protease inhibitor cocktail tablets (Roche), incubated on a rotating wheel for 2 h at 4°C and sonicated twice for 15 s. Afterwards, the lysate was centrifuged at 16,000 ***g*** for 30 min at 4°C. The cleared lysates were used to determine total protein amount using the Pierce BCA Protein Assay Kit (Thermo Fisher Scientific) according to the manufacturer's protocol. Proteins were separated on 4-12% Bis-Tris Protein Gels (NuPage Novex, Thermo Fisher Scientific) and transferred to nitrocellulose membrane (Whatman). The membrane was blocked with 5% BSA, 0.1% Tween-20, TBS for 1 h at room temperature. The primary antibody diluted in the blocking solution was incubated overnight at 4°C with continuous shaking. The membranes were washed 3× for 15 min with TBST (0.05% Tween-20, TBS) and incubated with secondary horseradish peroxidase-conjugated antibody for 1.5 h at room temperature. After washing with TBST, proteins were visualized using chemiluminescence (KPL). The following primary antibodies and dilution factors were used: anti-Raptor (2280S, Cell Signaling Technology, 1:1000), anti-phospho-S6 ribosomal protein (Ser235/236) (2211S, Cell Signaling Technology, 1:1000), anti-S6 ribosomal protein (2217S, Cell Signaling Technology, 1:1000), anti-phospho-4E-BP1 (Ser65) (9451S, Cell Signaling Technology, 1:1000), anti-phospho-4E-BP1 (9452S, Cell Signaling Technology, 1:1000), anti-α-actinin (A7732, Sigma-Aldrich, 1:5000), anti-Rictor (9476S, Cell Signaling Technology, 1:1000), anti-PKCα (2056S, Cell Signaling Technology, 1:1000), anti-phospho-PKCα (Ser657) (sc-12356, Santa Cruz Biotechnology, 1:500), anti-Akt (9272S, Cell Signaling Technology, 1:1000), anti-phospho-Akt (Ser473) (4058S, Cell Signaling Technology, 1:1′000). The secondary antibodies used were: anti-rabbit HRP and anti-mouse HRP (Jackson ImmunoResearch; 1:10000).

RNA extraction and qRT-PCR

Total RNA was extracted from whole E11.5 and E13.5 embryos or from hindlimb and foreleg muscles of E18.5 embryos using the RNeasy Mini Kit (Qiagen) according to the manufacturer's protocol. RNA was transcribed into cDNA using the iScript cDNA Synthesis Kit (Bio-Rad). Selected genes were amplified and detected using the Power SYBR Green PCR Master Mix (Applied Biosystems) and the relative gene expression was determined with the Step One software (ThermoFisher Scientific) and normalized to *Actb* expression. All qPCR primers are listed in Table S5.

Statistical analysis

All experiments were performed on a minimum of three independent biological samples indicated by the *n*. In all graphs, data are presented as mean±s.e.m. Statistical significance was determined using Student's *t*-test when two groups were compared, or using one or two-way ANOVA with Tukey's or Sidak's multiple comparisons test when more than two groups were compared. $P<0.05$ was considered statistically significant.

Acknowledgements

We thank the Biozentrum In-house FACS Core Facility, in particular Janine Boegli and Stella Stefanova, and the Imaging Core Facility, in particular Dr Kai Schleicher and Nikolaus Ehrenfeuchter, for technical support. MyoD1 (clone c-20) antibodies were obtained from Dr Valérie Allamand as a gift. MHC, Pax7 and myogenin antibodies were obtained from DSHB (Iowa, USA).

Competing interests

The authors declare no competing or financial interests.

Author contributions

Conceptualization: N.R., P.C., S.L., J.R.R., M.A.R.; Methodology: N.R., P.C., S.L., J.R.R.; Validation: N.R., L.E.; Formal analysis: N.R., L.E., C.E.; Investigation: N.R., L.E.; Resources: M.A.R.; Data curation: N.R., M.A.R.; Writing - original draft: N.R., P.C., M.A.R.; Writing - review & editing: N.R., P.C., S.L., L.E., J.R.R., C.E., M.A.R.; Visualization: N.R., M.A.R.; Supervision: P.C., S.L., J.R.R., M.A.R.; Project administration: M.A.R.; Funding acquisition: M.A.R.

Funding

This work was supported by the Canton of Basel-Stadt and the Canton of Basel-Landschaft, grants from the Schweizerischer Nationalfonds zur Förderung der Wissenschaftlichen Forschung (to M.A.R. and P.C.) and a Biozentrum PhD Fellowship (to N.R.).

Supplementary information

Supplementary information available online at
http://dev.biologists.org/lookup/doi/10.1242/dev.172460.supplemental

References

Bentzinger, C. F., Romanino, K., Cloëtta, D., Lin, S., Mascarenhas, J. B., Oliveri, F., Xia, J., Casanova, E., Costa, C. F., Brink, M. et al. (2008). Skeletal muscle-specific ablation of raptor, but not of rictor, causes metabolic changes and results in muscle dystrophy. *Cell Metab.* **8**, 411-424.

Biressi, S., Molinaro, M. and Cossu, G. (2007). Cellular heterogeneity during vertebrate skeletal muscle development. *Dev. Biol.* **308**, 281-293.

Blandino-Rosano, M., Barbaresso, R., Jimenez-Palomares, M., Bozadjieva, N., Werneck-De-Castro, J. P., Hatanaka, M., Mirmira, R. G., Sonenberg, N., Liu, M., Rüegg, M. A. et al. (2017). Loss of mTORC1 signalling impairs beta-cell homeostasis and insulin processing. *Nat. Commun.* **8**, 16014.

Bonneau, A. M. and Sonenberg, N. (1987). Involvement of the 24-kDa cap-binding protein in regulation of protein synthesis in mitosis. *J. Biol. Chem.* **262**, 11134-11139.

Carnio, S., Loverso, F., Baraibar, M. A., Longa, E., Khan, M. M., Maffei, M., Reischl, M., Canepari, M., Loefler, S., Kern, H. et al. (2014). Autophagy impairment in muscle induces neuromuscular junction degeneration and precocious aging. *Cell Rep.* **8**, 1509-1521.

Castets, P., Lin, S., Rion, N., Di Fulvio, S., Romanino, K., Guridi, M., Frank, S., Tintignac, L. A., Sinnreich, M. and Ruegg, M. A. (2013). Sustained activation of mTORC1 in skeletal muscle inhibits constitutive and starvation-induced autophagy and causes a severe, late-onset myopathy. *Cell Metab.* **17**, 731-744.

Cloetta, D., Thomanetz, V., Baranek, C., Lustenberger, R. M., Lin, S., Oliveri, F., Atanasoski, S. and Ruegg, M. A. (2013). Inactivation of mTORC1 in the developing brain causes microcephaly and affects gliogenesis. *J. Neurosci.* **33**, 7799-7810.

Comai, G., Sambasivan, R., Gopalakrishnan, S. and Tajbakhsh, S. (2014). Variations in the efficiency of lineage marking and ablation confound distinctions between myogenic cell populations. *Dev. Cell* **31**, 654-667.

Conejo, R. and Lorenzo, M. (2001). Insulin signaling leading to proliferation, survival, and membrane ruffling in C2C12 myoblasts. *J. Cell. Physiol.* **187**, 96-108.

Coolican, S. A., Samuel, D. S., Ewton, D. Z., Mcwade, F. J. and Florini, J. R. (1997). The mitogenic and myogenic actions of insulin-like growth factors utilize distinct signaling pathways. *J. Biol. Chem.* **272**, 6653-6662.

Crist, C. G., Montarras, D. and Buckingham, M. (2012). Muscle satellite cells are primed for myogenesis but maintain quiescence with sequestration of Myf5 mRNA targeted by microRNA-31 in mRNP granules. *Cell Stem Cell* **11**, 118-126.

Cuenda, A. and Cohen, P. (1999). Stress-activated protein kinase-2/p38 and a rapamycin-sensitive pathway are required for C2C12 myogenesis. *J. Biol. Chem.* **274**, 4341-4346.

Deries, M. and Thorsteinsdóttir, S. (2016). Axial and limb muscle development: dialogue with the neighbourhood. *Cell. Mol. Life Sci.* **73**, 4415-4431.

Dowling, R. J. O., Topisirovic, I., Alain, T., Bidinosti, M., Fonseca, B. D., Petroulakis, E., Wang, X., Larsson, O., Selvaraj, A., Liu, Y. et al. (2010). mTORC1-mediated cell proliferation, but not cell growth, controlled by the 4E-BPs. *Science* **328**, 1172-1176.

Dumont, N. A., Bentzinger, C. F., Sincennes, M. C. and Rudnicki, M. A. (2015). Satellite cells and skeletal muscle regeneration. *Comp. Physiol.* **5**, 1027-1059.

Erbay, E. and Chen, J. (2001). The mammalian target of rapamycin regulates C2C12 myogenesis via a kinase-independent mechanism. *J. Biol. Chem.* **276**, 36079-36082.

Erbay, E., Park, I.-H., Nuzzi, P. D., Schoenherr, C. J. and Chen, J. (2003). IGF-II transcription in skeletal myogenesis is controlled by mTOR and nutrients. *J. Cell Biol.* **163**, 931-936.

Fujita, R. and Crist, C. (2018). Translational control of the myogenic program in developing, regenerating, and diseased skeletal muscle. *Curr. Top. Dev. Biol.* **126**, 67-98.

Gangloff, Y.-G., Mueller, M., Dann, S. G., Svoboda, P., Sticker, M., Spetz, J.-F., Um, S. H., Brown, E. J., Cereghini, S., Thomas, G. and et al. (2004). Disruption of the mouse mTOR gene leads to early postimplantation lethality and prohibits embryonic stem cell development. *Mol. Cell. Biol.* **24**, 9508-9516.

Garcia-Prat, L., Martinez-Vicente, M., Perdiguero, E., Ortet, L., Rodríguez-UBREVA, J., Rebollo, E., Ruiz-Bonilla, V., Gutarra, S., Ballestar, E., Serrano, A. L. et al. (2016). Autophagy maintains stemness by preventing senescence. *Nature* **529**, 37-42.

Ge, Y. and Chen, J. (2012). Mammalian target of rapamycin (mTOR) signaling network in skeletal myogenesis. *J. Biol. Chem.* **287**, 43928-43935.

Ge, Y., Wu, A.-L., Warnes, C., Liu, J., Zhang, C., Kawasome, H., Terada, N., Boppart, M. D., Schoenherr, C. J. and Chen, J. (2009). mTOR regulates skeletal muscle regeneration in vivo through kinase-dependent and kinase-independent mechanisms. *Am. J. Physiol. Cell Physiol.* **297**, C1434-C1444.

Ge, Y., Yoon, M. S. and Chen, J. (2011). Raptor and Rheb negatively regulate skeletal myogenesis through suppression of insulin receptor substrate 1 (IRS1). *J. Biol. Chem.* **286**, 35675-35682.

Gensch, N., Borchardt, T., Schneider, A., Riethmacher, D. and Braun, T. (2008). Different autonomous myogenic cell populations revealed by ablation of Myf5-expressing cells during mouse embryogenesis. *Development* **135**, 1597-1604.

Goodman, C. A. and Hornberger, T. A. (2013). Measuring protein synthesis with SUnSET: a valid alternative to traditional techniques? *Exerc. Sport Sci. Rev.* **41**, 107-115.

Guertin, D. A., Stevens, D. M., Thoreen, C. C., Burds, A. A., Kalaany, N. Y., Moffat, J., Brown, M., Fitzgerald, K. J. and Sabatini, D. M. (2006). Ablation in mice of the mTORC components raptor, rictor, or mLST8 reveals that mTORC2 is required for signaling to Akt-FOXO and PKCalpha, but not S6K1. *Dev. Cell* **11**, 859-871.

Haldar, M., Karan, G., Tvrdik, P. and Capecchi, M. R. (2008). Two cell lineages, myf5 and myf5-independent, participate in mouse skeletal myogenesis. *Dev. Cell* **14**, 437-445.

Haller, S., Kapuria, S., Riley, R. R., O'leary, M. N., Schreiber, K. H., Andersen, J. K., Melov, S., Que, J., Rando, T. A., Rock, J. et al. (2017). mTORC1 Activation during Repeated Regeneration Impairs Somatic Stem Cell Maintenance. *Cell Stem Cell* **21**, 806-818.e5.

Hung, C.-M., Calejman, C. M., Sanchez-Gurmaches, J., Li, H., Clish, C. B., Hettmer, S., Wagers, A. J. and Guertin, D. A. (2014). Rictor/mTORC2 loss in the Myf5 lineage reprograms brown fat metabolism and protects mice against obesity and metabolic disease. *Cell Rep.* **8**, 256-271.

Kleinert, M., Parker, B. L., Chaudhuri, R., Fazakerley, D. J., Serup, A., Thomas, K. C., Krycer, J. R., Sylow, L., Fritzen, A. M., Hoffman, N. J. et al. (2016). mTORC2 and AMPK differentially regulate muscle triglyceride content via Perilipin 3. *Mol. Metab.* **5**, 646-655.

Martinez-Lopez, N., Athonvarangkul, D., Sahu, S., Coletto, L., Zong, H., Bastie, C. C., Pessin, J. E., Schwartz, G. J. and Singh, R. (2013). Autophagy in Myf5+ progenitors regulates energy and glucose homeostasis through control of brown fat and skeletal muscle development. *EMBO Rep.* **14**, 795-803.

Miyabara, E. H., Conte, T. C., Silva, M. T., Baptista, I. L., Bueno, C., Jr, Fiamoncini, J., Lambertucci, R. H., Serra, C. S., Brum, P. C., Pithon-Curi, T. et al. (2010). Mammalian target of rapamycin complex 1 is involved in differentiation of regenerating myofibers in vivo. *Muscle Nerve* **42**, 778-787.

Mozzetta, C., Consalvi, S., Saccone, V., Tierney, M., Diamantini, A., Mitchell, K. J., Marazzi, G., Borsellino, G., Battistini, L., Sassoon, D. et al. (2013). Fibroadipogenic progenitors mediate the ability of HDAC inhibitors to promote regeneration in dystrophic muscles of young, but not old Mdx mice. *EMBO Mol. Med.* **5**, 626-639.

Murakami, M., Ichisaka, T., Maeda, M., Oshiro, N., Hara, K., Edenhofer, F., Kiyama, H., Yonezawa, K. and Yamanaka, S. (2004). mTOR is essential for growth and proliferation in early mouse embryos and embryonic stem cells. *Mol. Cell. Biol.* **24**, 6710-6718.

Murphy, M. M., Lawson, J. A., Mathew, S. J., Hutcheson, D. A. and Kardon, G. (2011). Satellite cells, connective tissue fibroblasts and their interactions are crucial for muscle regeneration. *Development* **138**, 3625-3637.

Ott, M. O., Bober, E., Lyons, G., Arnold, H. and Buckingham, M. (1991). Early expression of the myogenic regulatory gene, myf-5, in precursor cells of skeletal muscle in the mouse embryo. *Development* **111**, 1097-1107.

Pallafacchina, G., Blaauw, B. and Schiaffino, S. (2013). Role of satellite cells in muscle growth and maintenance of muscle mass. *Nutr. Metab. Cardiovasc. Dis.* **23** Suppl. 1, S12-S18.

Park, I. H. and Chen, J. (2005). Mammalian target of rapamycin (mTOR) signaling is required for a late-stage fusion process during skeletal myotube maturation. *J. Biol. Chem.* **280**, 32009-32017.

Pasut, A, Oleynik, P. and Rudnicki, M. A. (2012). Isolation of muscle stem cells by fluorescence activated cell sorting cytometry. *Methods Mol. Biol.* **798**, 53-64.

Pollard, H. J., Willett, M. and Morley, S. J. (2014). mTOR kinase-dependent, but raptor-independent regulation of downstream signaling is important for cell cycle exit and myogenic differentiation. *Cell Cycle* **13**, 2517-2525.

Ramirez-Valle, F., Badura, M. L., Braunstein, S., Narasimhan, M. and Schneider, R. J. (2010). Mitotic raptor promotes mTORC1 activity, G(2)/M cell cycle progression, and internal ribosome entry site-mediated mRNA translation. *Mol. Cell. Biol.* **30**, 3151-3164.

Risson, V., Mazelin, L., Roceri, M., Sanchez, H., Moncollin, V., Corneloup, C., Richard-Bulteau, H., Vignaud, A., Baas, D., Defour, A. et al. (2009). Muscle inactivation of mTOR causes metabolic and dystrophin defects leading to severe myopathy. *J. Cell Biol.* **187**, 859-874.

Rodgers, J. T., King, K. Y., Brett, J. O., Cromie, M. J., Charville, G. W., Maguire, K. K., Brunson, C., Mastey, N., Liu, L., Tsai, C. R. et al. (2014). mTORC1 controls the adaptive transition of quiescent stem cells from G0 to G(Alert). *Nature* **510**, 393-396.

Rosenblatt, J. D., Lunt, A. I., Parry, D. J. and Partridge, T. A. (1995). Culturing satellite cells from living single muscle fiber explants. *In Vitro Cell. Dev. Biol. Animal* **31**, 773-779.

Sarbassov, D. D., Ali, S. M., Sengupta, S., Sheen, J. H., Hsu, P. P., Bagley, A. F., Markhard, A. L. and Sabatini, D. M. (2006). Prolonged rapamycin treatment inhibits mTORC2 assembly and Akt/PKB. *Mol. Cell* **22**, 159-168.

Saxton, R. A. and Sabatini, D. M. (2017). mTOR signaling in growth, metabolism, and disease. *Cell* **168**, 960-976.

Schneider, S. (2013). Skeletal examination by double staining for ossified bone and cartilaginous tissue. *Methods Mol. Biol.* **947**, 215-221.

Seale, P., Bjork, B., Yang, W., Kajimura, S., Chin, S., Kuang, S., Scimè, A., Devarakonda, S., Conroe, H. M., Erdjument-Bromage, H. et al. (2008). PRDM16 controls a brown fat/skeletal muscle switch. *Nature* **454**, 961-967.

Sonenberg, N. and Hinnebusch, A. G. (2009). Regulation of translation initiation in eukaryotes: mechanisms and biological targets. *Cell* **136**, 731-745.

Tallquist, M. D., Weismann, K. E., Hellstrom, M. and Soriano, P. (2000). Early myotome specification regulates PDGFA expression and axial skeleton development. *Development* **127**, 5059-5070.

Tchorz, J. S., Suply, T., Ksiazek, I., Giachino, C., Cloëtta, D., Danzer, C. P., Doll, T., Isken, A., Lemaistre, M., Taylor, V. et al. (2012). A modified RMCE-compatible Rosa26 locus for the expression of transgenes from exogenous promoters. *PLoS ONE* **7**, e30011.

Tintignac, L. A., Brenner, H.-R. and Rüegg, M. A. (2015). Mechanisms regulating neuromuscular junction development and function and causes of muscle wasting. *Physiol. Rev.* **95**, 809-852.

Uezumi, A., Fukada, S., Yamamoto, N., Takeda, S. and Tsuchida, K. (2010). Mesenchymal progenitors distinct from satellite cells contribute to ectopic fat cell formation in skeletal muscle. *Nat. Cell Biol.* **12**, 143-152.

Vinagre, T., Moncaut, N., Carapuço, M., Nóvoa, A., Bom, J. and Mallo, M. (2010). Evidence for a myotomal Hox/Myf cascade governing nonautonomous control of rib specification within global vertebral domains. *Dev. Cell* **18**, 655-661.

White, R. B., Biérinx, A.-S., Gnocchi, V. F. and Zammit, P. S. (2010). Dynamics of muscle fibre growth during postnatal mouse development. *BMC Dev. Biol.* **10**, 21.

Zismanov, V., Chichkov, V., Colangelo, V., Jamet, S., Wang, S., Syme, A., Koromilas, A. E. and Crist, C. (2016). Phosphorylation of eIF2alpha is a translational control mechanism regulating muscle stem cell quiescence and self-renewal. *Cell Stem Cell* **18**, 79-90.

Supplementary Information

Supplementary Figures

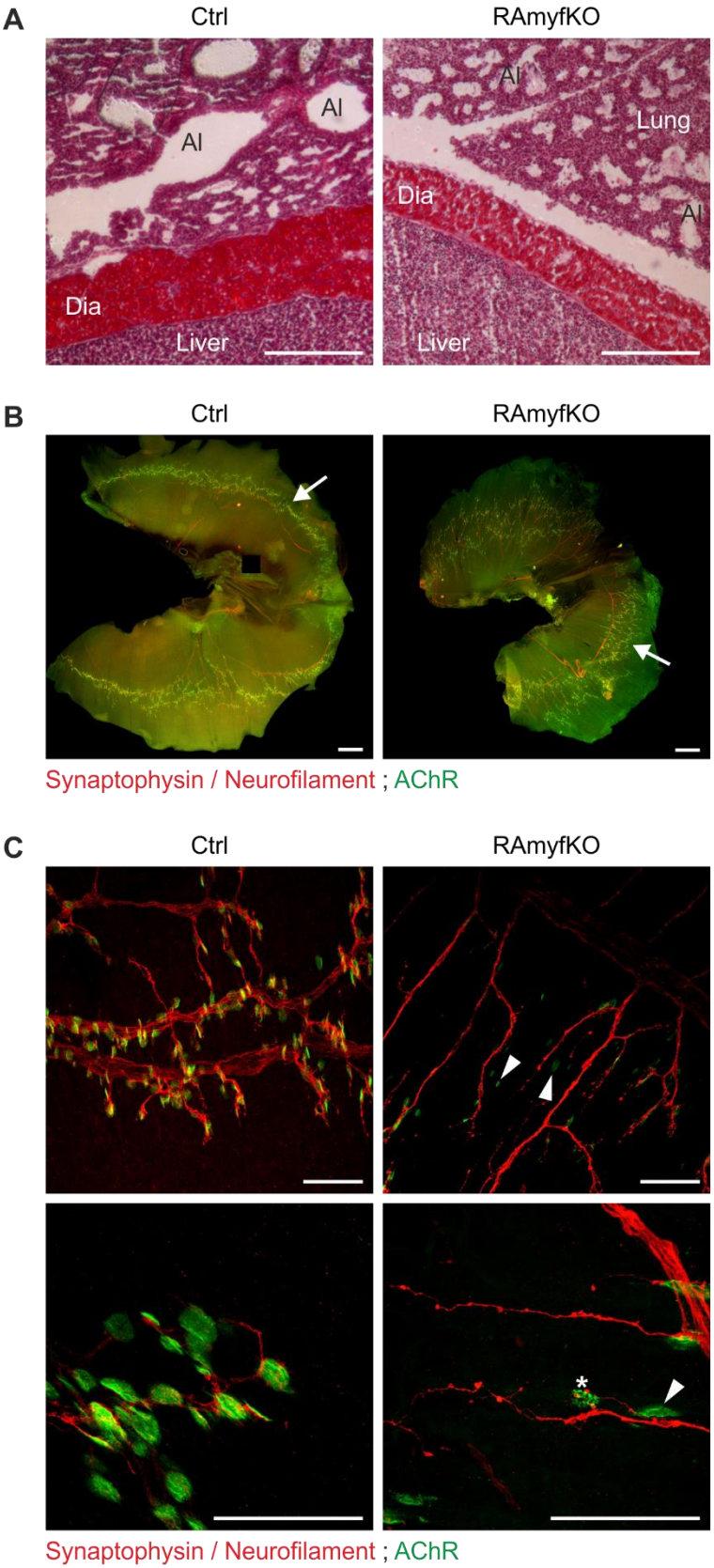

Figure S1. RAmyfKO embryos die perinatally due to respiratory failure

(A) H&E coloration of longitudinal sections of newborn pups (P0) in the region of the lung, diaphragm (Dia) and liver. Alveoli (Al) are small and collapsed, and the interstitial mesenchyme is thicker in RAmyfKO compared to Ctrl lungs, indicating that their lungs were never inflated. Diaphragm thickness is reduced in RAmyfKO mice. Scale bar, 500 µm.

(B and C) Whole-mount preparation of E17.5 diaphragms were stained with antibodies against synaptophysin and neurofilament (red), which stain the presynaptic motor nerve, and with fluorescently labeled α-bungarotoxin (green), which stains acetylcholine receptors (AChR). Compared to controls, the innervation zone (B, arrows) in RAmyfKO embryos is widened and disorganized. AChR aggregates are rarely innervated (C, arrowheads) and motor axons continue to grow over the entire length of the muscle. Fragmented postsynaptic AChR clusters in RAmyfKO diaphragms are indicated with an asterisk. Scale bar, 500 µm (B) and 50 µm (C).

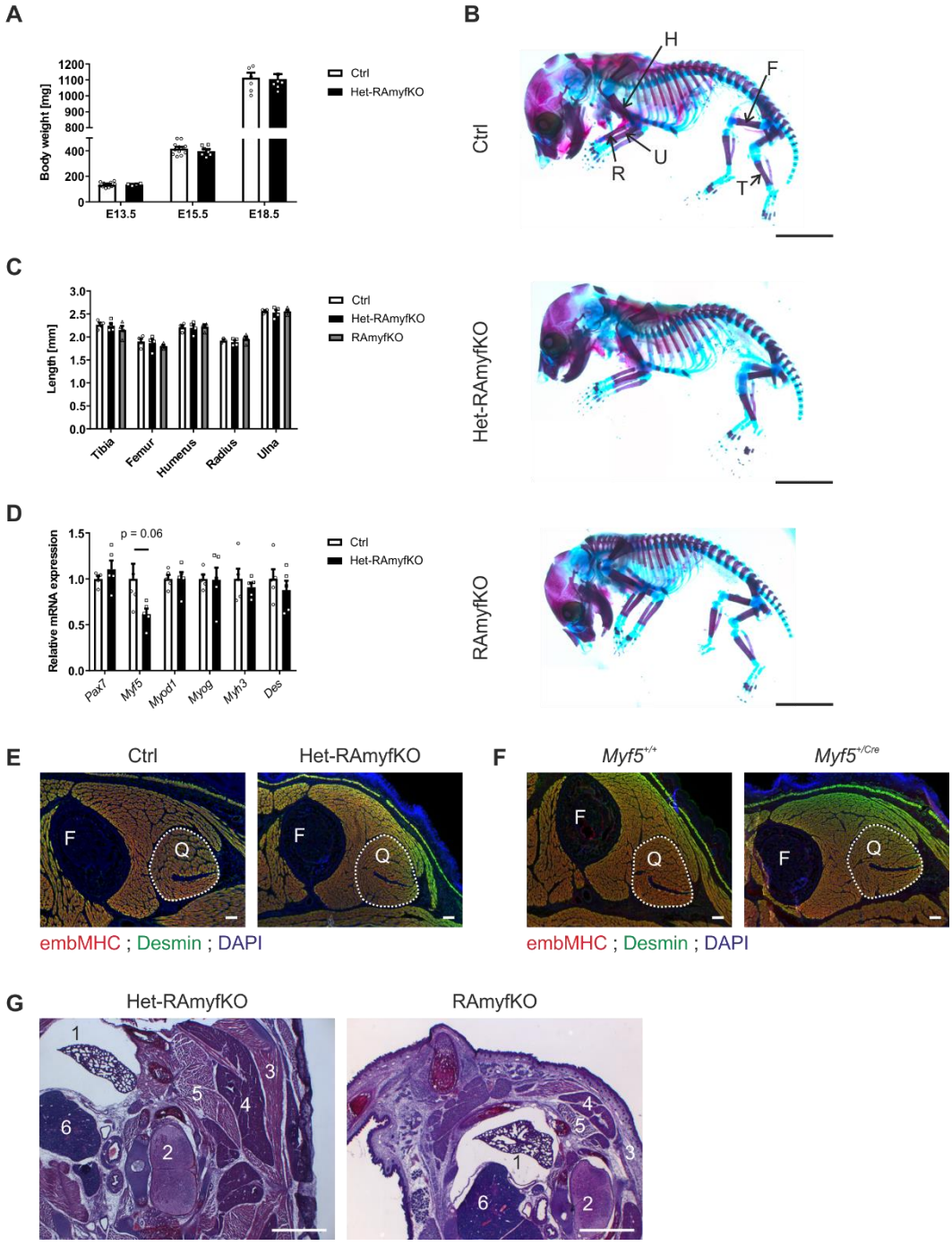

Figure S2. Het-RAmyfKO embryos do not show defects in embryonic muscle development

(A) Body weight of Ctrl (*Myf5*$^{+/+}$*; Rptor*$^{fl/fl}$) and Het-RAmyfKO (*Myf5*$^{+/Cre}$*; Rptor*$^{+/fl}$) embryos at the indicated embryonic stages (n = 11/12/7 Ctrl and 4/7/7 Het-RAmyfKO embryos at E13.5/15.5/18.5).

(B) Alcian blue (cartilage) and alizarin red (ossified bones) staining of E18.5 embryos of the genotypes indicated. T, tibia; F, femur; H, humerus; R, radius; U, ulna. Scale bar, 5 mm.

(C) Quantification of bone length in the different embryos (n = 4; except Ctrl Radius, n=3).

(D) mRNA levels of the indicated genes in E18.5 hindlimb muscle from control (Ctrl) and Het-RAmyfKO (*Myf5*$^{+/Cre}$*; Rptor*$^{+/fl}$) embryos. Gene expression is normalized to *Actb* levels (n = 5). Note that in Het-RAmyfKO embryos, all genes measured (except of *Myf5*) are expressed at the same level as in Ctrl.

(E and F) Immunostaining against embMHC (red) and desmin (green) of cross-sections of E18.5 Ctrl and Het-RAmyfKO embryos (E) and *Myf5*$^{+/+}$ and *Myf5*$^{+/Cre}$ embryos (F) in the region of the quadriceps muscle. F, femur; Q, quadriceps (delineated with dotted lines). Scale bar, 100 µm.

(G) H&E coloration of cross-sections through the upper part of E18.5 embryos. 1, lung; 2, spinal cord; 3, trapezius muscle; 4, brown fat; 5, semispinalis muscles; 6, thymus. Scale bar, 1000 µm.

Data represented as mean ± SEM. Student's *t* test and one-way ANOVA with Tukey's multiple comparisons test.

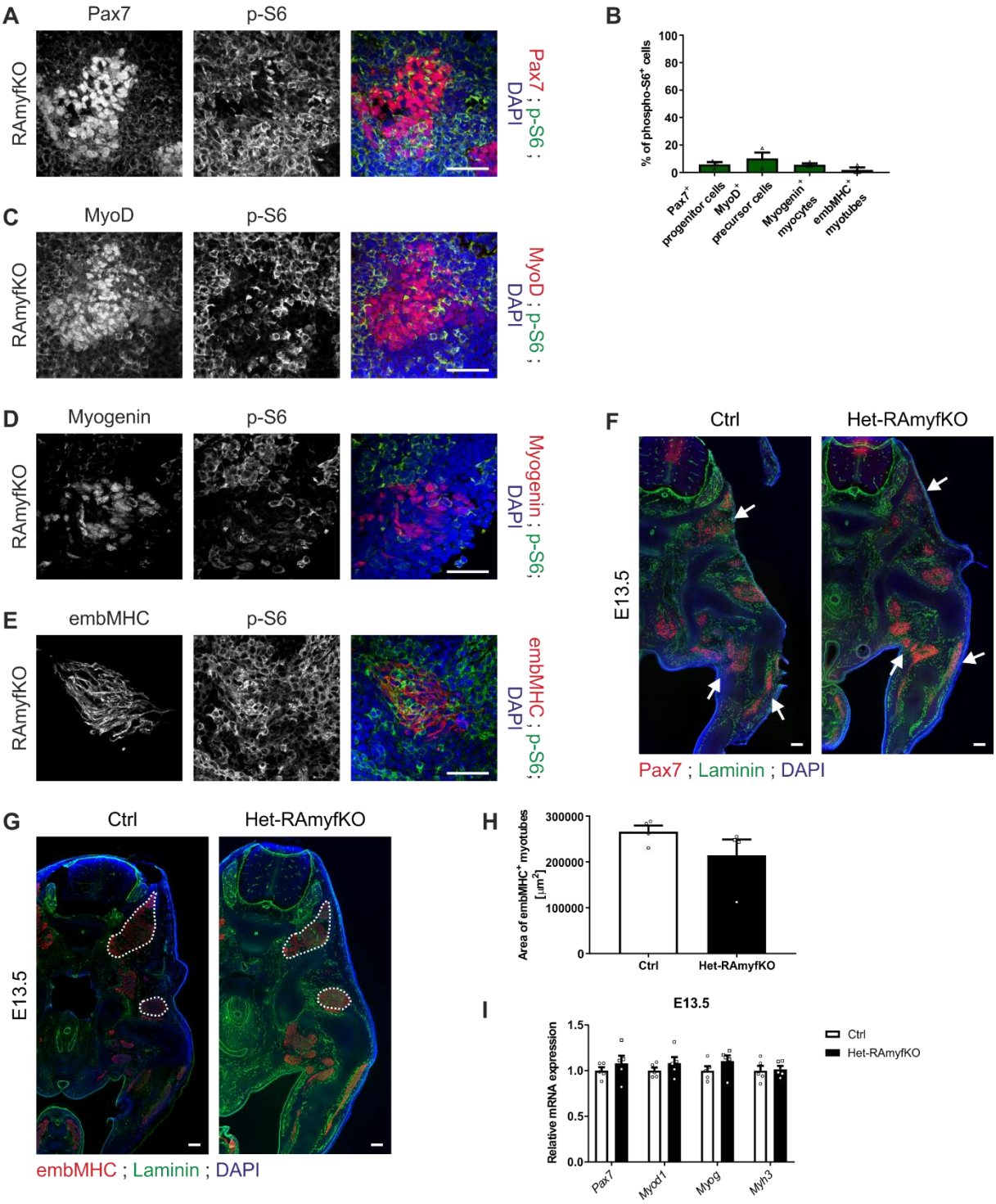

Figure S3. Effect of raptor depletion on myogenesis and mTORC1 signaling

(A, C - E) Immunostaining against phospho-S6 Ser235/236 and Pax7 (A), MyoD (C), myogenin (D), embMHC (E) on cross-sections of E11.5 RAmyfKO embryos. Strong phospho-S6 staining is detectable in non-myogenic cells. Scale bar, 50 µm.

(B) Percentage of phospho-S6-positive muscle progenitors ($Pax7^+$), precursors ($MyoD^+$), myocytes ($Myogenin^+$) and myotubes ($embMHC^+$) (n = 3).

(F and G) Immunostaining against Pax7 (red, F) or embMHC (red, G) and laminin (green) of cross-sections of E13.5 Ctrl and Het-RAmyfKO embryos. Arrows in F point to muscle progenitors in the dermomyotome and hindlimbs. Dotted lines in G indicated the myotome and the quadriceps (embMHC-positive region). Scale bar, 100 µm.

(H) Quantification of the area of the myotome in E13.5-old Ctrl and Het-RAmyfKO embryos (n = 4).

(I) Relative mRNA levels of *Pax7*, *Myod1*, *Myog* and *Myh3* in E13.5 Ctrl and Het-RAmyfKO embryos. Normalization to *Actb* levels (n = 5).

Data represented as mean ± SEM. Student's *t* test.

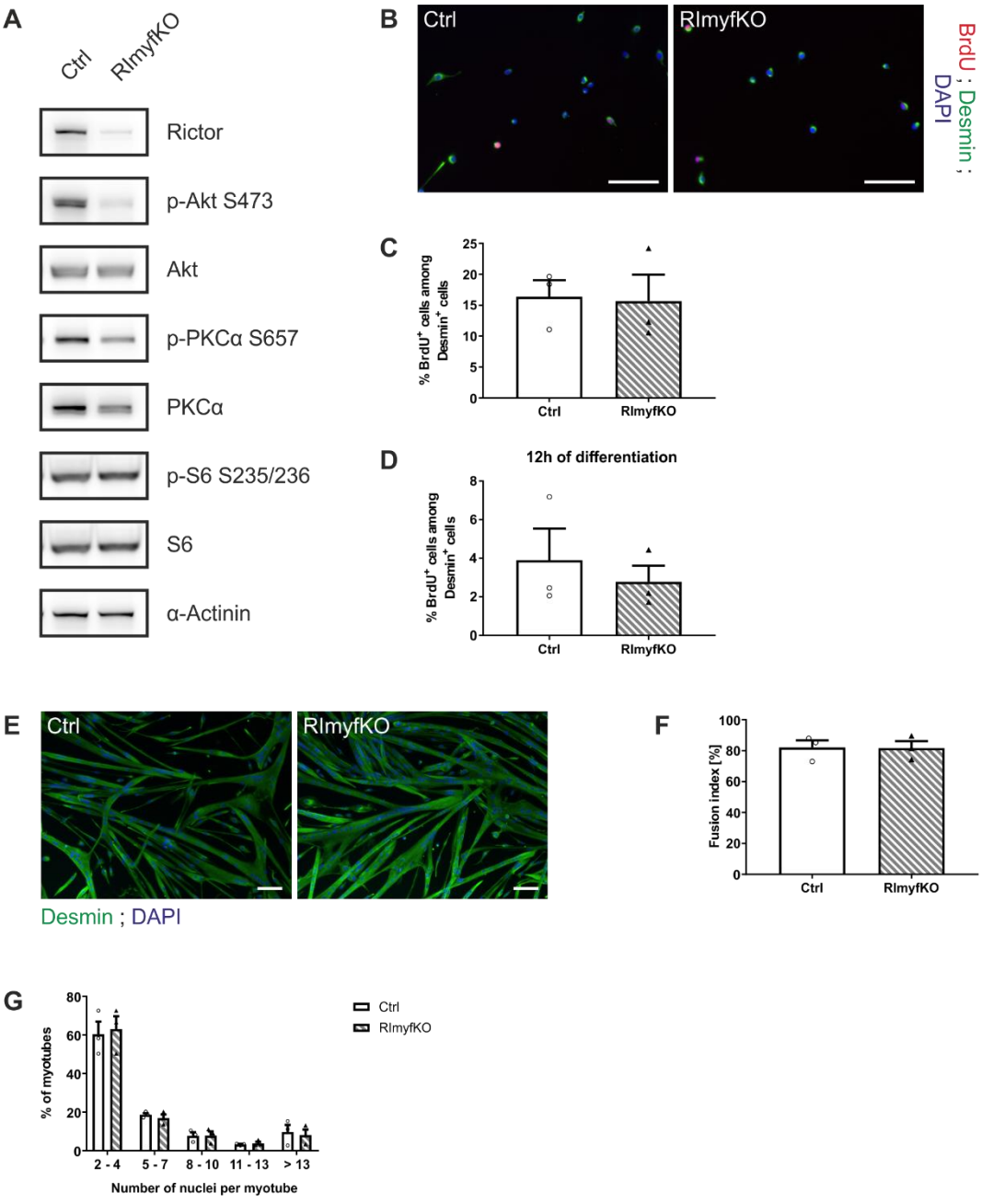

Figure S4. mTORC2 signaling is dispensable for the proliferation, differentiation and fusion of myoblasts

Primary myoblasts were isolated from EDL muscle of 2-3 week-old Ctrl or RImyfKO mice and cultured in growth or differentiation media.

(A) Western blot analysis using lysates from proliferating Ctrl and RImyfKO primary myoblasts using antibodies against the proteins indicated. Myoblasts isolated from RImyfKO muscle are depleted for rictor and show decreased mTORC2 signaling. α-actinin was used as loading control (n = 3). See also Table S2.

(B) Immunostaining against BrdU (red) and desmin (green) labels the myoblasts being in the S-phase during the 1 h BrdU pulse. Scale bar, 50 µm.

(C and D) Percentage of $BrdU^+$ / $Desmin^+$ myoblasts after 48 h of proliferation (C) or 12 h of differentiation (D) (n = 3).

(E) Immunostaining of myotubes against desmin (green) after 48 h of differentiation. Scale bar, 100 µm.

(F and G) Fusion index (F) and relative frequency of myotubes containing the indicated number of myonuclei (G) of Ctrl and RImyfKO myotubes after 48 h in differentiation medium are not different (n = 3).

Data represented as mean ± SEM. Student's *t* test.

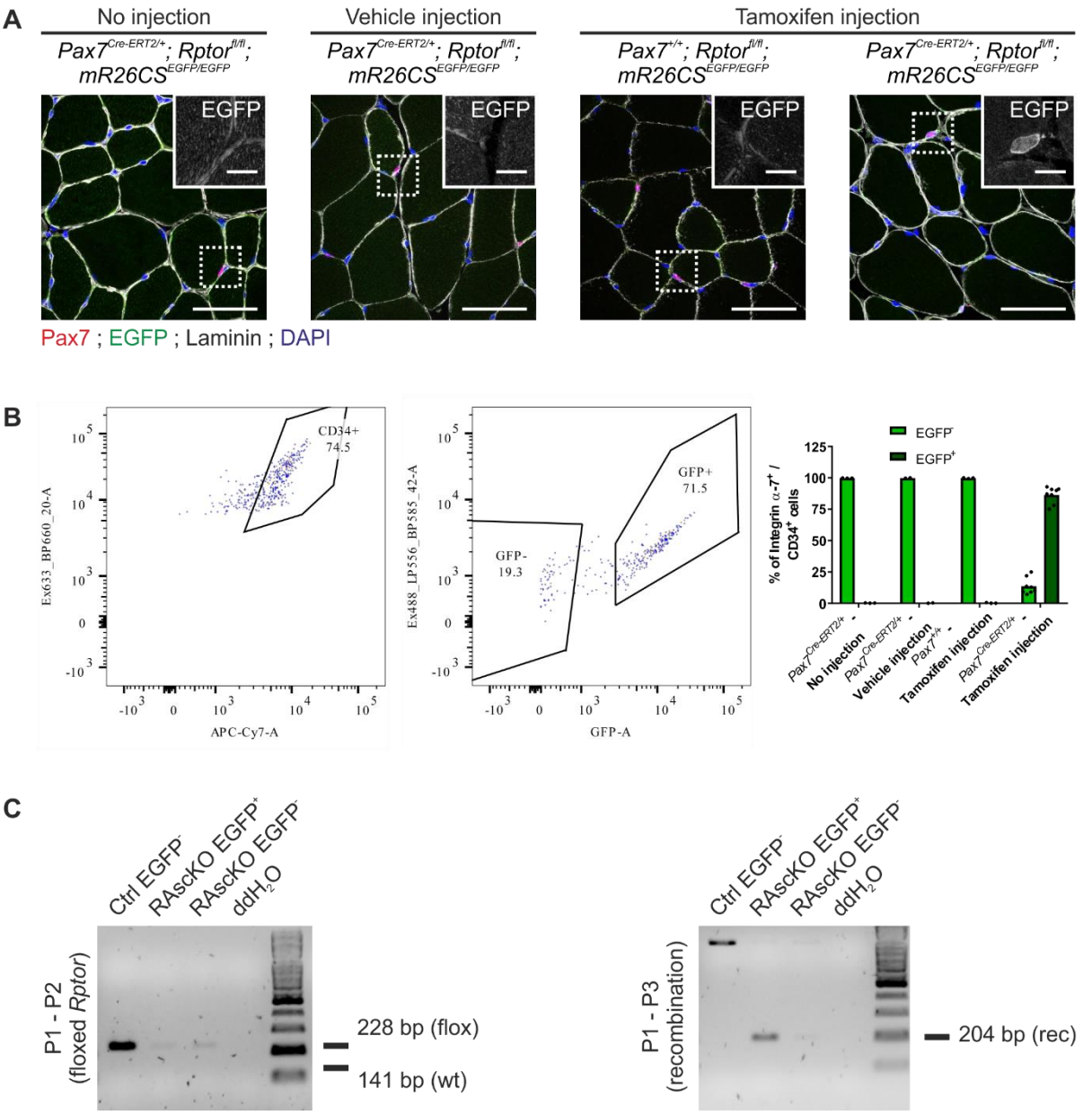

Figure S5. EGFP labels raptor-depleted satellite cells of RAscKO mice

(A) Immunostaining against Pax7 (red), EGFP (green) and laminin (grey) of TA muscle cross-sections from Ctrl and RAscKO mice after vehicle or tamoxifen treatment. Scale bar, 50 µm and 10 µm (inset).

(B) Representative FACS cytometry blots from hindlimb and foreleg muscles from 3-month-old RAscKO mice, 10 days after tamoxifen treatment. Cells were selected based on their lineage-low (Sca1, CD45, CD31, CD11b; PE, Ex561, not shown), Integrin α7-high (APC, not shown), CD34-high (Alexa-647, Ex633) and EGFP-high signals. All satellite cells isolated from Ctrl (*Pax7*$^{+/+}$; *Rptor*$^{fl/fl}$; *mR26CS*$^{EGFP/EGFP}$) and RAscKO (*Pax7*$^{Cre-Ert2/+}$; *Rptor*$^{fl/fl}$;

mR26CS$^{EGFP/EGFP}$) mice treated with / without tamoxifen, respectively, appeared as EGFP-negative. 86.4 % of the satellite cells isolated from tamoxifen-treated RAscKO mice were EGFP-positive (n=2 *Pax7*$^{Cre\text{-}Ert2/+}$ Vehicle; 3 *Pax7*$^{Cre\text{-}Ert2/+}$ No injection; 3 *Pax7*$^{+/+}$ Tamoxifen; 8 *Pax7*$^{Cre\text{-}Ert2/+}$ Tamoxifen).

(C) PCR analysis of freshly FACS-isolated satellite cells using primers to distinguish between the wild-type (wt, 141 bp), floxed (flox, 228 bp) or recombined (rec, 204 bp) *Rptor* alleles. In Ctrl satellite cells, the floxed *Rptor* allele was detected, while in RAscKO satellite cells, the recombined *Rptor* allele was amplified (n = 3).

Data represented as mean.

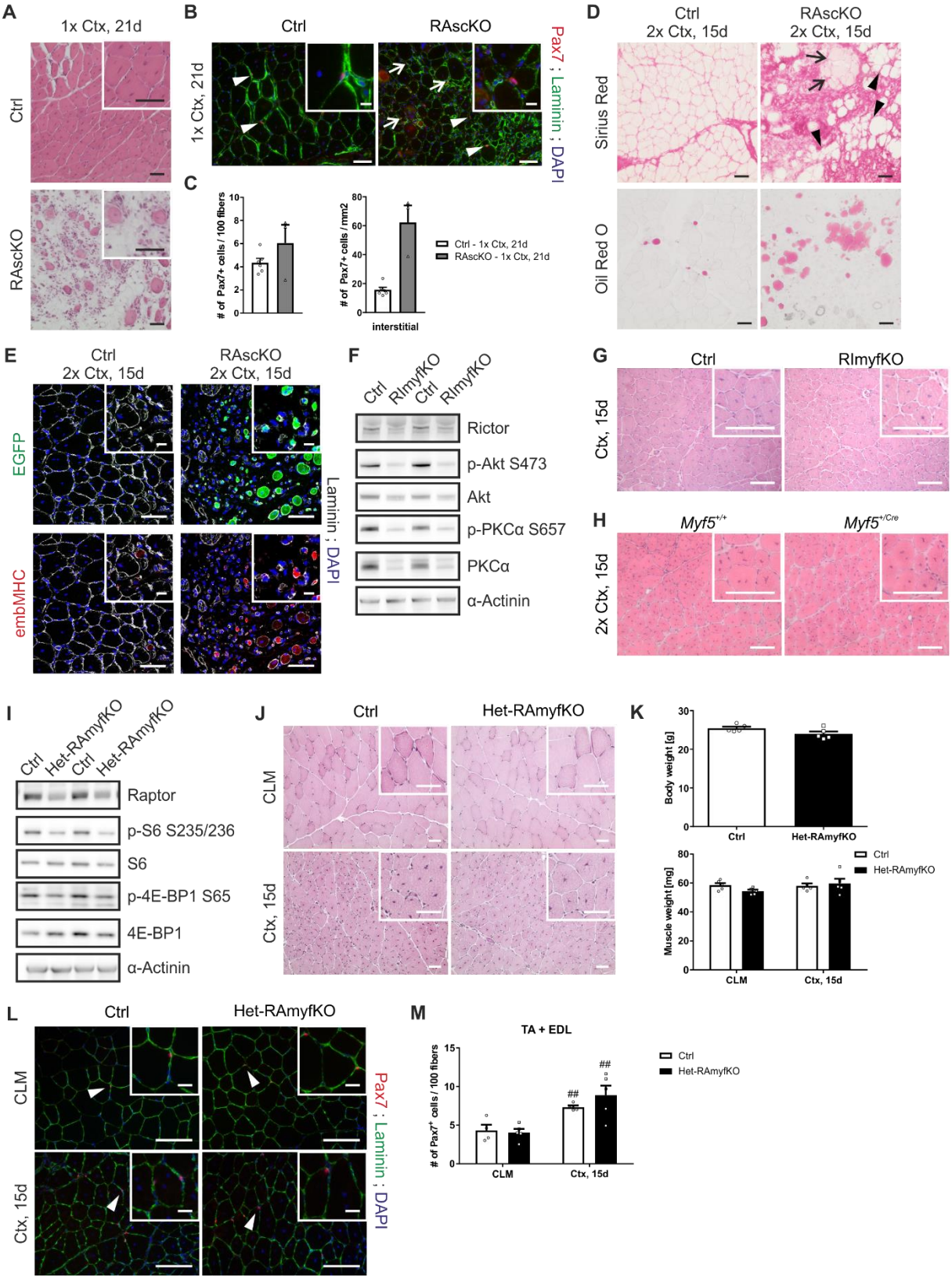

Figure S6. Loss of mTORC1, but not the inactivation of mTORC2 or 50 % reduction in raptor protein levels, affects muscle regeneration at young age

(A) H&E coloration of regenerating TA from Ctrl and RAscKO mice, 21 days after one injury (1x Ctx, 15d). Scale bar, 50 µm.

(B) Immunostaining against Pax7 (red) and laminin (green) on TA muscle cross-sections from Ctrl and RAscKO mice 21 days post-injury. Arrowheads and arrows point to sub-laminar and interstitial Pax7-positive satellite cells, respectively. Scale bar, 50 µm (10 µm for insets).

(C) The number of sub-laminar and interstitial Pax7-positive cells in TA muscle was counted and normalized to 100 myofibers or per area unit (mm^2). Counting was performed 21 days post-injury (n = 6 Ctrl and 3 RAscKO mice).

(D) Sirius Red and Oil Red O colorations on regenerating TA muscles from Ctrl and RAscKO mice, 15 days after the 2nd Ctx-induced injury (2x Ctx, 15d). Injured RAscKO muscle shows accumulation of fibrotic tissue and lipid droplets. In the top panel, arrows and arrowheads point to regenerating fibers and fat accumulation, respectively. Scale bar, 50 µm.

(E) Immunostaining against EGFP (green) or embMHC (red) and laminin (grey) on regenerating TA muscle of Ctrl and RAscKO mice 15 days after two injuries (2x Ctx, 15d). While regeneration is complete in Ctrl muscle, injured RAscKO muscle shows very rare regenerating fibers. Scale bar, 50 µm and 10 µm at higher magnification.

(F) Western blot analysis of TA muscle from 5-month-old Ctrl (*Myf5*$^{+/+}$*; Rictor*$^{fl/fl}$) and RImyfKO (*Myf5*$^{+/Cre}$*; Rictor*$^{fl/fl}$) mice using antibodies against the proteins indicated. An equal amount of proteins was loaded in each lane. α-actinin was used as loading control (n = 5).

(G) H&E coloration of injured TA (Ctx, 15d) from Ctrl and RImyfKO mice. Regenerating fibers are characterized by their centralized nuclei. Scale bar, 50 µm.

(H) H&E coloration of regenerating TA from *Myf5*$^{+/+}$ and *Myf5*$^{+/Cre}$ mice after two successive rounds of Ctx-induced injuries (2x Ctx, 15d). Scale bar, 50 µm.

(I) Western blot analysis of contralateral (CLM), non-injured gastrocnemius muscle from 3-month-old Ctrl (*Myf5*$^{+/+}$*; Rptor*$^{fl/fl}$) and Het-RAmyfKO (*Myf5*$^{+/Cre}$*; Rptor*$^{+/fl}$) mice using antibodies against the proteins indicated. An equal amount of proteins was loaded in each lane. α-actinin was used as loading control (n = 5).

(J) H&E coloration of CLM and injured TA (Ctx, 15d) from Ctrl and Het-RAmyfKO mice. Scale bar, 50 µm.

(K) Body and muscle weight of 3-month-old Ctrl and Het-RAmyfKO mice was measured 15 days after cardiotoxin- (Ctx) induced muscle damage. Restoration of the muscle mass following injury compared to the non-injured, muscle of the contralateral leg (CLM) indicates that muscle regeneration was efficient in Het-RAmyfKO mice (n = 5).

(L) Immunostaining against Pax7 (red) and laminin (green) of CLM or injured (Ctx, 15d) TA muscles to visualize quiescent satellite cells underneath the basal lamina (arrowhead). Scale bar, 100 µm and 20 µm at higher magnification.

(M) Number of Pax7-positive satellite cells normalized to 100 myofibers in uninjured and injured TA muscles of Ctrl and Het-RAmyfKO mice (n = 4 Ctrl and 5 Het-RAmyfKO mice).

Data represented as mean ± SEM. ## $p < 0.01$, compared to uninjured muscle, Student's *t* test.

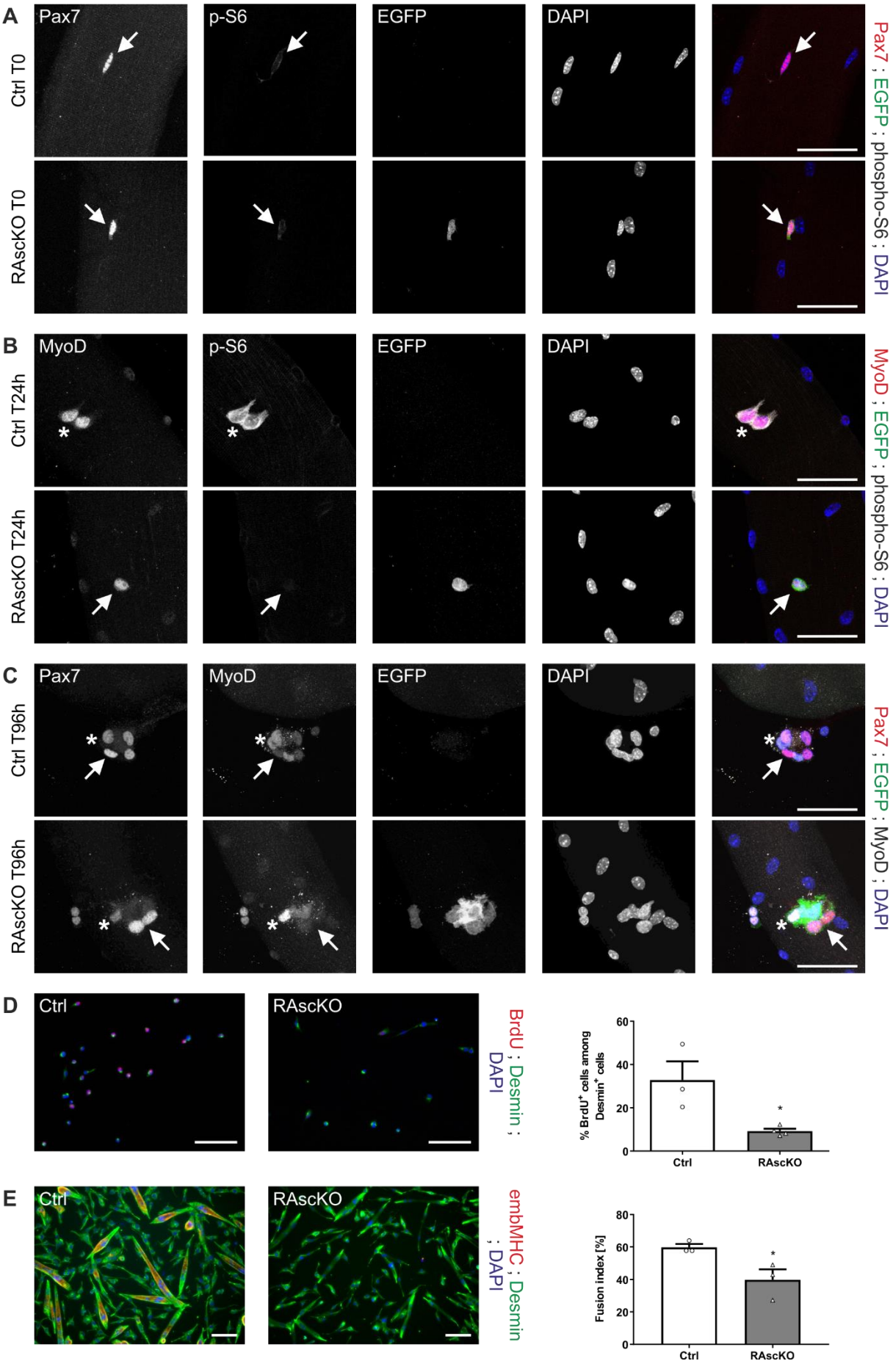

Figure S7. Characterization of RAscKO satellite cells *in vitro*

(A - C) Single myofibers were isolated from Ctrl and RAscKO EDL muscles 10 days after tamoxifen treatment and their associated satellite cells analyzed directly after isolation (T0), after 24 h (T24h) or 96 h (T96h) in culture. (A and B) Immunostaining against Pax7 (red, A) or MyoD (red, B), EGFP (green) and phospho-S6 (grey) of satellite cells on Ctrl and RAscKO myofibers at T0 (A) or T24h (B). Ctrl, but not RAscKO satellite cells show low (arrow, A) and high (asterix, B) S6 phosphorylation at T0 and T24h, respectively. (C) Immunostaining against Pax7 (red), EGFP (green) and MyoD (grey) of satellite cells from Ctrl and RAscKO mice at T96h. Like in control culture, RAscKO satellite cell colonies contain cells that entered differentiation ($Pax7^-$; $MyoD^+$, asterix) and some that returned into quiescence ($Pax7^+$; $MyoD^-$, arrow) at T96h. Scale bar, 50 µm.

(D) FACS-sorted satellite cells (Ctrl $EGFP^-$, RAscKO $EGFP^+$) were cultured in growth media for 48 h and BrdU-labeled 1 h before fixation. Immunostaining against BrdU (red) and desmin (green) visualizes the myoblasts that are in the S-phase of the cell cycle during the pulse. Right: Proportion of BrdU-positive cells in the myoblast population (n = 3 Ctrl and 4 RAscKO). Scale bar, 100 µm.

(E) Immunostaining against embMHC (red) and desmin (green) of myotubes after 4 days in differentiation medium. Right: Fusion index of the cells for the different genotypes (n = 3). Scale bar, 100 µm.

Data represented as mean ± SEM. * $p < 0.05$, Student's *t* test.

Supplementary Tables

	Ctrl	RAmyfKO
Phospho-PKCα Ser657	100 ± 9	89 ± 4
PKCα	100 ± 4	96 ± 29

Table S1. Quantification of Western blot analysis in hindlimb muscle from E18.5 Ctrl and RAmyfKO embryos

Protein levels were quantified in hindlimb muscle from E18.5 Ctrl and RAmyfKO embryos. The total amount of proteins was adjusted according to concentration. Data are represented as the average of grey values ± SEM, after background subtraction and normalization to α-actinin and to values from Ctrl mice (n = 6 Ctrl; 5 (for PKCα) and 3 (for p-PKCα) RAmyfKO embryos). Student's *t* test.

	Ctrl	RImyfKO
Rictor	100 ± 11	10 ± 6 **
Phospho-PKCα Ser657	100 ± 38	30 ± 6
PKCα	100 ± 28	38 ± 16
Phospho-Akt Ser473	100 ± 25	18 ± 4 *
Akt	100 ± 32	66 ± 6
Phospho-S6 Ser235/236	100 ± 40	70 ± 6
S6	100 ± 26	79 ± 11

Table S2. Quantification of Western blot analysis of primary myoblasts isolated from EDL muscle of Ctrl and RImyfKO mice

Protein levels were quantified in primary myoblasts isolated from EDL muscle of 2-3 week-old Ctrl and RImyfKO mice. The total amount of proteins was adjusted according to concentration. Data are represented as the average of grey values ± SEM, after background subtraction and normalization to α-actinin and to values from Ctrl mice (n = 3). * $p < 0.05$, ** $p < 0.05$, Student's *t* test.

	TA muscle	
	Ctrl	RImyfKO
Rictor	100 ± 9	72 ± 6 *
Phospho-Akt Ser473	100 ± 12	18 ± 2 ***
Akt	100 ± 7	76 ± 9
Phospho-PKCα Ser657	100 ± 22	31 ± 2 *
PKCα	100 ± 10	29 ± 2 ***

Table S3. Quantification of Western blot analysis in TA muscle from 5-month-old Ctrl and RImyfKO mice

Protein levels were quantified in TA muscle from 5 month-old Ctrl and RImyfKO mice. The total amount of proteins was adjusted according to concentration. Data are represented as the average of grey values ± SEM, after background subtraction and normalization to α-actinin and to values from Ctrl mice (n = 5). * $p < 0.05$, *** $p < 0.001$, Student's *t* test.

	Quadriceps muscle	
	Ctrl	Het-RAmyfKO
Raptor	100 ± 15	58 ± 9 *
Phospho-S6 Ser235/236	100 ± 23	61 ± 13
S6	100 ± 6	106 ± 24
Phospho-4E-BP1 Ser65	100 ± 18	80 ± 15
4E-BP1	100 ± 11	115 ± 34

Table S4. Quantification of Western blot analysis in Quadriceps muscle from 3 month-old Ctrl and Het-RAmyfKO mice

Protein levels were quantified in uninjured quadriceps muscle from 3-month-old Ctrl and Het-RAmyfKO mice. The total amount of proteins was adjusted according to concentration. Data are represented as the average of grey values ± SEM, after background subtraction and normalization to α-actinin and to values from Ctrl mice (n = 5). * $p < 0.05$, Student's *t* test.

	Forward primer	Reverse primer
Pax7	GAG GTG ACA GGA GGC AGA AG	AGC TGC CAG CAA GAT GGT AT
Myf5	AGG AAA AGA AGC CCT GAA GC	GCA AAA AGA ACA GGC AGA GG
Myod1	CAT TCC AAC CCA CAG AAC CT	TGC TGT CTC AAA GGA GCA GA
Myog	ACT CCC TTA CGT CCA TCG TG	CAG GAC AGC CCC ACT TAA AA
Myh3	GCA CGA AGA AGC CAA GAT TC	TCA GCT GCT CGA TCT CTT CA
Des	GAG GTT GTC AGC GAG GCT AC	CTT CAG GAG GCA GTG AGG AC
Actb	CAG CTT CTT TGC AGC TCC TT	GCA GCG ATA TCG TCA TCC A

Table S5. Primers used for quantitative PCR analysis

Supplementary Materials and Methods

Isolation of embryonic and adult muscle progenitors by FACS

Isolation of embryonic myogenic cells by FACS was adapted from (Pasut et al., 2012). In brief, hindlimb and foreleg muscles of E18.5 embryos were dissected and minced. Digestion of the tissue was started by transferring the muscle pieces into PBS with Collagenase B (2.5 U/ml, Roche) and Dispase II (2.5 U/ml, Roche) at 37 °C for 40 min with repeated trituration using a FBS-coated pipette. Digestion was stopped by the addition of 2 volumes of 10 % FBS. The cell suspension was filtered with a 70 µm cell strainer (Corning) and centrifuged two times at 500 g for 5 min. Adult muscle stem cells were isolated from hindlimb and foreleg muscles of 3 month-old mice 10 days after tamoxifen treatment according to a protocol modified from (Garcia-Prat et al., 2016). Muscles were minced and digested in PBS with 0.16 % Collagenase B (Roche) and 0.125% Trypsin (Gibco) at 37 °C under rotating conditions. After 25 min, the supernatant was collected, enzyme-inactivated with 0.25 volume of FBS and filtered with a 70 µm cell strainer (Corning). The remaining muscle pieces were again digested at 37 °C under rotating conditions. This procedure was repeated 4 times until the entire muscle was digested. The collected cell suspension was centrifuged at 60 g for 10 min to remove big pieces, the pellet washed and re-centrifuged. Supernatants were centrifuged at 500 g for 15 min to collect isolated cells. Single cells were incubated with the following antibodies: anti-Integrin α-7 (MBL International Corporation), biotin anti-CD34 (eBioscience), PE anti-CD11b (eBioscience), PE anti-CD45 (eBioscience), PE anti-Ly-6A/E (BD Biosciences), PE anti-CD31 (BD Biosciences), APC-Cy7 Streptavidin (BD Biosciences) and Alexa647 anti-mouse IgG1 (Molecular Probes). Additionally, DAPI was used as viability marker. Embryonic (Integrin α-7^+/$CD11b^-$/$CD45^-$/$Sca1^-$/$CD31^-$) and adult (Integrin α-7^+/$CD34^+$/$CD11b^-$/$CD45^-$/$Sca1^-$/$CD31^-$) myogenic cells were sorted with FACSAria IIIu cell sorter (BD Biosciences) and analyzed using the FlowJo V10 (FlowJo) software. Cells expressing EGFP were sorted based on their endogenous fluorescence.

Supplementary References

BENTZINGER, C. F., ROMANINO, K., CLOETTA, D., LIN, S., MASCARENHAS, J. B., OLIVERI, F., XIA, J., CASANOVA, E., COSTA, C. F., BRINK, M., ZORZATO, F., HALL, M. N. & RUEGG, M. A. 2008. Skeletal muscle-specific ablation of raptor, but not of rictor, causes metabolic changes and results in muscle dystrophy. *Cell metabolism,* 8**,** 411-24.

GARCIA-PRAT, L., MARTINEZ-VICENTE, M., PERDIGUERO, E., ORTET, L., RODRIGUEZ-UBREVA, J., REBOLLO, E., RUIZ-BONILLA, V., GUTARRA, S., BALLESTAR, E., SERRANO, A. L., SANDRI, M. & MUNOZ-CANOVES, P. 2016. Autophagy maintains stemness by preventing senescence. *Nature,* 529**,** 37-42.

PASUT, A., OLEYNIK, P. & RUDNICKI, M. A. 2012. Isolation of muscle stem cells by fluorescence activated cell sorting cytometry. *Methods Mol Biol,* 798**,** 53-64.

SCHNEIDER, S. 2013. Skeletal examination by double staining for ossified bone and cartilaginous tissue. *Methods Mol Biol,* 947**,** 215-21.

TCHORZ, J. S., SUPLY, T., KSIAZEK, I., GIACHINO, C., CLOETTA, D., DANZER, C. P., DOLL, T., ISKEN, A., LEMAISTRE, M., TAYLOR, V., BETTLER, B., KINZEL, B. & MUELLER, M. 2012. A modified RMCE-compatible Rosa26 locus for the expression of transgenes from exogenous promoters. *PLoS One,* 7**,** e30011.